

INSIGHTS INTO THE BEHAVIOR OF PRECIOUS METALS IN PRIMITIVE, S-UNDERSATURATED MAGMAS: EVIDENCE FROM THE HEAZLEWOOD RIVER COMPLEX, TASMANIA

DAVID C. PECK* AND REID R. KEAYS

Department of Geology, University of Melbourne, Parkville, Victoria 3052, Australia

ABSTRACT

The Heazlewood River mafic-ultramafic complex (HRC) comprises several sequences of primitive layered ultramafic cumulates, gabbroic dykes and Mg-rich volcanic suites, including boninite and low-Ti tholeiitic basalt. The volcanic suites are considered to have been cogenetic with the parental liquids for the cumulate sequences, and represent second-stage melts derived from depleted mantle in an island-arc setting. These liquids contained extremely low abundances of S and remained S-undersaturated throughout the crystallization of the complex. The distribution of precious metals in the HRC reflects several basic geochemical properties of the platinum-group elements (*PGE*) and Au. Osmium, Ir and Ru are concentrated into primitive olivine-chromite adcumulates. Palladium, Au and, to a lesser degree, Pt, are progressively enriched in more evolved rock-types and appear to have been partitioned into residual liquids during fractional crystallization. The relative compatibility of the precious metals during crystallization of the HRC was: Os > Ir > Ru > Pt > Au > Pd. One locality contains cumulates that are selectively enriched in Pt, but the processes responsible for this spatial anomaly have not been ascertained. The complex is not a likely prospect for stratiform *PGM* - sulfide mineralization because the parental magmas, despite being extremely fertile, failed to attain S-saturation. However, the observed enrichment of Os, Ir and Ru in primitive dunites from the western part of the HRC, and the presence of spatially associated alluvial "osmiridium" occurrences, may be related to the crystallization of cumulus Os-Ir ± Ru alloys. The relative abundances of the precious metals in the HRC is most comparable to cumulates from ophiolites. The documented behavior of the *PGE* and Au during the development of the HRC should be applicable to other intrusions having affinities with second-stage melts.

Keywords: boninite, geochemistry, "osmiridium", platinum-group elements, precious metals, second-stage melt, ultramafic intrusion, Heazlewood River Complex, Tasmania.

SOMMAIRE

Le complexe mafique-ultramafique de Heazlewood River, en Tasmanie, comprend plusieurs séquences litées

*Present address: Centre in Mining and Mineral Exploration Research, Laurentian University, Sudbury, Ontario P3E 2C6.

de cumulats ultramafiques primitifs, de dykes gabbroïques, et de suites volcaniques magnésiennes qui contiennent boninite et basalte tholéïitique à faible teneur en Ti. Les suites volcaniques seraient cogénétiques avec les liquides qui ont donné la séquence de cumulats, et représenteraient des magmas de seconde génération dérivés d'un manteau géochimiquement appauvri dans un milieu d'arc insulaire. Ces liquides contiennent des teneurs en S très faibles, et sont demeurés sous-saturés en S tout au long de la cristallisation du complexe. La distribution des métaux précieux résulte de plusieurs propriétés géochimiques des éléments du groupe du platine (*EGP*) et de l'or. Parmi ceux-ci, Os, Ir et Ru sont concentrés dans les adcumulats primitifs à olivine + chromite. Par contre, Pd, Au et, à un degré moindre, Pt s'enrichissent progressivement dans les membres les plus évolués, et semblent avoir été concentrés dans les liquides résiduels au cours de la cristallisation fractionnée. La compatibilité relative des métaux précieux au cours de la cristallisation semble avoir été Os > Ir > Ru > Pt > Au > Pd. A un endroit, nous avons découvert des cumulats enrichis en Pt, mais les processus qui sont à l'origine de cet enrichissement localisé n'ont pas été définis. Le complexe n'est pas propice à la prospection d'une minéralisation stratiforme en *EGP* et en sulfures parce que les magmas parentaux, quoique très fertiles, n'ont pas réussi à atteindre la saturation en S. Toutefois, l'enrichissement observé des *EGP* du groupe de l'iridium dans les dunites primitives de la partie occidentale du complexe, ainsi que la présence d'"osmiridium" dans les alluvions de la région, pourraient bien témoigner de la cristallisation d'un alliage Os-Ir ± Ru dans les cumulats. Les abondances relatives des métaux précieux dans le complexe de Heazlewood River ressemblent beaucoup à celles des séquences de cumulats dans les ophiolites. Le comportement des *EGP* et de l'or que nous avons documenté s'appliquerait à tout complexe dans lequel il est question de magmas formés au cours d'une deuxième fusion du manteau.

(Traduit par la Rédaction)

Mots-clés: boninite, géochimie, "osmiridium", éléments du groupe du platine, métaux précieux, magma de seconde génération, complexe intrusif ultramafique, complexe de Heazlewood River, Tasmanie.

INTRODUCTION

Whereas most recent geochemical studies of the platinum-group elements (*PGE*) in mafic and ultramafic intrusions have focussed on *PGE* mineraliza-

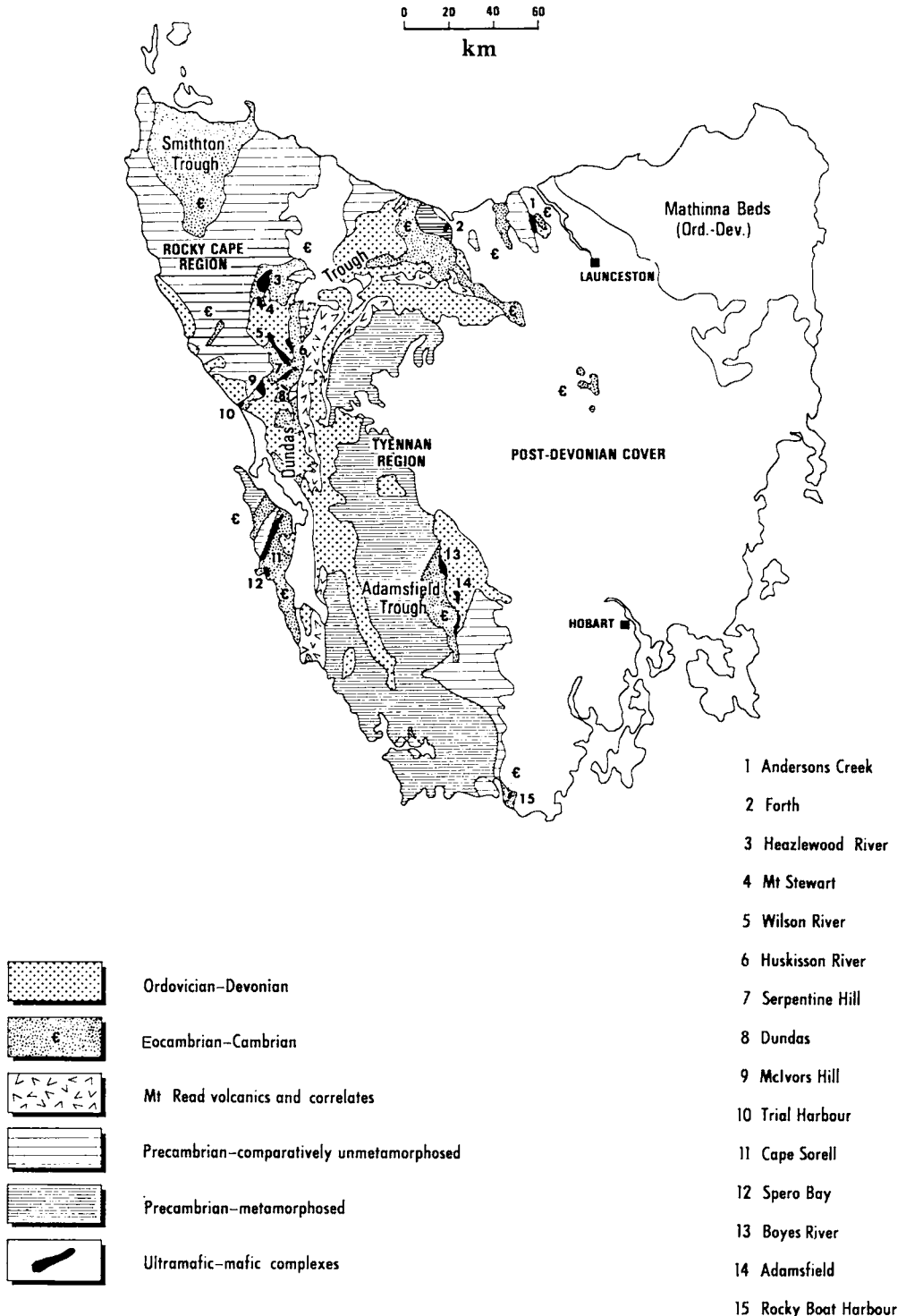


FIG. 1. Generalized geology of western Tasmania. Numbers (1-15) refer to mafic-ultramafic complexes. Taken with permission from Brown (1986); modified after Williams (1978).

tion within the intrusions, there persists a paucity of information relating to the distribution of these metals in unmineralized rocks. This paper redresses the problem in that it presents new geochemical data for the Heazlewood River mafic-ultramafic complex (HRC), Tasmania, which was formed from magmas that remained sulfur-undersaturated throughout the crystallization of the cumulate sequences. An exception to this observation is reflected by the rare development of *PGM*-bearing chromitites, representing very localized increases in the S tenor of the parental magmas for the complex.

Therefore, in contrast to the majority of ultramafic intrusions, which were formed at least in part from S-saturated magmas, the HRC provides an ideal opportunity to study the behavior of the *PGE* and Au in a S-impoverished system. In addition, the influence of chromitite development in the HRC on the distribution of the *PGE* is known from a recently completed investigation (Peck & Keays 1990). Distribution patterns for the *PGE* are examined, and new observations pertaining to the behavior of the precious metals during fractional crystallization, partial melting and low-temperature alteration are presented. The results also provide important insights into the genesis of spatially associated alluvial Os-Ir alloys and place constraints on the tectonic setting and petrogenesis of the HRC.

REGIONAL GEOLOGICAL SETTING

The Heazlewood River mafic-ultramafic complex is the largest of several such complexes that occur within Cambrian volcano-sedimentary troughs in western Tasmania (Fig. 1). The HRC occurs within the Dundas Trough, which comprises Eocambrian and Cambrian volcanic and sedimentary sequences and contains the majority of the ultramafic complexes. Detailed accounts of the geology of western Tasmania are given by Williams (1978), Brown (1986), Corbett & Lees (1987) and Varne & Foden (1987).

The complexity of the Cambrian geology of western Tasmania has been attributed to both extensional tectonics (Williams 1978, Varne & Foden 1987) and compressional tectonics (Solomon & Griffiths 1972, Corbett & Lees 1987). Berry & Crawford (1988) have suggested that a collisional tectonic regime existed in the Early to Middle Cambrian and led to the emplacement of a low-angle thrust sheet containing the mafic-ultramafic complexes onto a passive continental margin assemblage. Brown & Jenner (1989) suggested that the geological and geochemical features of the Cambrian volcanic suites can be accounted for by a model involving arc-continent collision in the early Late Cambrian. Analogies have been drawn between the geological configuration of

western Tasmania and the ophiolite terranes of Oman and Newfoundland (Berry & Crawford 1988).

The mafic-ultramafic complexes are small (<50 km²) allochthonous bodies that were tectonically emplaced during the Middle Cambrian (Brown 1986). The most detailed descriptions of the complexes are given by Rubenach (1973) and Brown (1986). General features of the complexes include the predominance of olivine and orthopyroxene cumulates, locally abundant gabbroic dykes, and an association between the cumulates and both a boninite and low-titanium tholeiitic basalt suite. Calculations presented by Brown (1986) suggest that the Tasmanian mafic-ultramafic complexes crystallized at temperatures of 1200–1300°C and pressures of between 2 and 5 kbar, consistent with high-level emplacement.

The complexes have previously been described as ophiolites and disrupted ophiolites (Rubenach 1973, 1974, Varne & Brown 1978, Varne & Foden 1987), ultramafic-gabbroic complexes (Rubenach 1973), cumulates formed in a crustal magma chamber and derived from boninitic and low-Ti tholeiitic basalt melts (Brown 1986) and, in the case of one complex (Serpentine Hill, No. 7, Fig. 1), as having similarities to Alaskan-type complexes (Brown *et al.* 1988). Recent studies (Berry & Crawford 1988, Brown & Jenner 1989) indicate that the Tasmanian mafic-ultramafic complexes are most analogous to those "ophiolites" considered to have formed in a supra-subduction zone environment (*e.g.*, the Troodos ophiolite). These bodies are characterized by the presence of low-Ti lavas and ultramafic cumulates enriched in Ca-poor pyroxene. Geochemical and petrological features of the Cambrian boninite and low-Ti tholeiitic basalt suites are consistent with their eruption in an island-arc environment (Brown & Jenner 1989).

Several of the complexes were mined for alluvial deposits of "osmiridium" (Os-Ir-Ru alloy). Approximately 31,000 ounces of the alloy were recovered between 1910 and 1954, and the HRC was the world's major supplier of Os and Ir from 1910 to 1920 (Jennings *et al.* 1967, Mertie 1969). The history of "osmiridium" mining in Tasmania was described by Twelvetrees (1914), Reid (1920) and Nye (1929). In a more recent study, Ford (1981) described the chemistry of these alloys and demonstrated that the majority of the grains are iridosmine and rutheniridosmine ($0.35 < \text{Os} < 0.51$; $0.31 < \text{Ir} < 0.43$; $0.06 < \text{Ru} < 0.29$; $\text{Pt} < 0.02$; $\text{Rh} < 0.02$; $\text{Fe} < 0.04$; atomic proportions). Brown *et al.* (1988) produced the first detailed investigation into the *PGE* geochemistry of the Tasmanian mafic-ultramafic complexes. A recently completed study by the present authors examined the *PGE*-chromitite occurrences in the Heazlewood River complex (Peck & Keays 1990).



REFERENCE

SEDIMENTARY AND VOLCANIC SEQUENCES

-  Tertiary
-  EoCambrian
-  Silurian-Devonian
-  Precambrian

HEAZLEWOOD RIVER MAFIC - ULTRAMAFIC COMPLEX
CUMULATE ULTRAMAFIC SEQUENCES







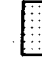

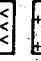
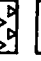





-  BRASSEY HILL HARZBURGITE SEQUENCE
 -  harzburgite with minor orthopyroxene and dunite
 -  PURCELL'S PLAIN LHERZOLITE SEQUENCE (plagioclase) dunite, herzoltite and harzburgite
 -  GABBRO HILL PLAGIOCLASE PYROXENITE SEQUENCE plagioclase orthopyroxene, harzburgite and dunite
 -  CAUDRY'S HILL ORTHOPYROXENITE SEQUENCE olivine orthopyroxene and plagioclase pyroxene
 -  FENTON'S SPUR PERIDOTITE SEQUENCE dunite, peridotite and orthopyroxene
 -  BRONZITE HILL ORTHOPYROXENITE SEQUENCE orthopyroxene with minor harzburgite
 -  NINETEEN MILE CREEK DUNITE SEQUENCE dunite with minor harzburgite and orthopyroxene
- MAFIC ROCKS
-  TONALITE COMPLEX tonalite, diorite and gabbro
 -  LOW-TI THOLEIITIC BASALT
 -  BONINITE
- geological boundary  fault
- hard rock workings  alluvial workings
- chromite occurrence  "osmiridium" occurrence 
- 0 km 1

Fig. 2. Generalized geology of the Heazlewood River mafic-ultramafic complex. Cumulate sequences were mapped by Rubenach (1973), Creneau (1980), and Brown (1986). Volcanic and sedimentary sequences were mapped by D. C. Peck (unpublished).

THE HEAZLEWOOD RIVER MAFIC-ULTRAMAFIC COMPLEX

The first detailed account of the geology of the HRC was presented by Twelvetrees (1914) as part of an investigation into the historic Bald Hill "osmiridium" field, which occurs in the western part of the complex (now known as Caudry's Hill). An excellent account of the history of "osmiridium" mining in the HRC is given by Reid (1920). More recent accounts of the geology of the HRC are given by Rubenach (1973), Creenaune (1980) and Mann (1988). The following description of the geology of the complex (Fig. 2) is based on the work of the present authors and previous workers.

The HRC is the largest and least-disrupted of the Tasmanian mafic-ultramafic complexes (Rubenach 1973) and outcrops over an area of 50 km². It is in faulted contact with Eocambrian - Early Devonian volcanic and sedimentary sequences, which suggests that it was affected by further tectonic activity after the initial Middle Cambrian emplacement (Rubenach 1973, Brown 1986). The complex consists of a maximum of 5 km of layered ultramafic cumulates and cross-cutting gabbroic rocks and up to 3 km of overlying low-Ti tholeiitic basalt and boninite (Fig. 2; Brown 1986). The HRC also hosts a tonalite complex and probable tectonic melanges (Creenaune 1980). Cumulate layering trends northeasterly, and dips are near-vertical. The complex is cut by numerous faults and shear zones, which commonly trend northwesterly to northerly. The faults are generally steeply dipping and sinistral. The cumulate rocks record variable degrees of serpentinization. Calcium metasomatism, pervasive serpentinization and talc-carbonate alteration are focussed along the faults and shear zones. Stratigraphic relationships within the complex are complicated by the presence of northeast-trending faults, which are parallel to the igneous layering. However, cryptic variations in mineral compositions (Peck & Keays, unpublished data) and local facies criteria (cross-bedding, cyclic units) indicate that the majority of the cumulate sequences are young to the southeast. A major north-trending fault divides the complex into western and eastern sections, with very little correlation between rock types across the fault (Fig. 2).

Western section

The western part of the HRC comprises medium-grained adcumulate dunite and subordinate harzburgite and orthopyroxenite of the 19 Mile Creek dunite sequence. The rocks are locally intensely deformed and display layer-parallel foliations that may have developed during the tectonic emplacement of the complex. This sequence is the only unit that occurs in both the western and eastern sections of the HRC.

It has long been considered to represent the primary source for the spatially associated alluvial occurrences of "osmiridium" (Twelvetrees 1914). Abandoned hard-rock workings are located in serpentinized dunite on the western side of Caudry's Hill (Fig. 2). The contact between the 19 Mile Creek dunite sequence and the Fenton's Spur peridotite sequence is a fault in the vicinity of Fenton's Spur, but is gradational in the southwestern part of Caudry's Hill. The latter sequence consists of a western succession containing adcumulate dunite, harzburgite and minor orthopyroxenite (Fenton's Spur dunite sequence) that is overlain by well-layered adcumulate dunite, harzburgite, lherzolite, wehrlite, orthopyroxenite and websterite (Fenton's Spur pyroxenite sequence). Faulting has occurred along the gradational contact between the Fenton's Spur peridotite sequence and the Caudry's Hill pyroxenite sequence. The latter comprises a basal series of massive, coarse-grained, adcumulate olivine orthopyroxenite with minor dunite interlayers (Caudry's Hill orthopyroxenite sequence) and an upper series of medium-grained mesocumulate plagioclase orthopyroxenite, plagioclase websterite and rare gabbroic rocks (Caudry's Hill plagioclase websterite sequence). The Gabbro Hill plagioclase pyroxenite sequence comprises a well-layered, coarse-grained, adcumulate dunite-harzburgite-orthopyroxenite succession (Gabbro Hill dunite sequence) that is intruded by massive, coarse-grained to pegmatitic plagioclase orthopyroxenite and plagioclase websterite (Gabbro Hill plagioclase orthopyroxenite sequence).

Eastern section

The nature of the contacts between the 19 Mile Creek dunite sequence, the Bronzite Hill orthopyroxenite sequence and the Purcell's Plain lherzolite sequence is unclear. The Bronzite Hill sequence is only observed in the northeastern part of the complex, and consists of massive, coarse-grained, adcumulate orthopyroxenite, with minor harzburgite interlayers. The Purcell's Plain lherzolite sequence comprises a western succession of interlayered adcumulate dunite, pyroxene dunite and harzburgite (Purcell's Plain dunite sequence) that has a gradational contact with an overlying, more extensive succession of well-layered, mesocumulate-textured plagioclase dunite and plagioclase lherzolite with subordinate plagioclase harzburgite, troctolite and anorthosite (Purcell's Plain plagioclase lherzolite sequence). The Purcell's Plain lherzolite sequence has a conformable contact with the Brassey Hill harzburgite sequence. The latter comprises interlayered sequences of dunite, poikilitic (plagioclase) harzburgite, adcumulate harzburgite, olivine orthopyroxenite and orthopyroxenite, which represent cyclic units of 20 - 50 m in thickness (Mann 1988).

Mafic dykes

Three suites of dykes are recognized within the cumulate sequences of the HRC, *viz.*, (1) fine-grained gabbro-norite, (2) medium-grained anorthosite, and (3) coarse-grained to pegmatitic gabbro-norite and plagioclase pyroxenite. The dykes are generally tabular and < 1 m thick, but larger bodies of fine-grained gabbro-norite, up to 200 m thick, also are observed. The dykes are most abundant in the eastern HRC, but also intrude the Gabbro Hill sequence and the eastern part of the Caudry's Hill

sequence. In addition, poorly exposed dykes of coarse-grained basaltic pyroxenite are found in spatial association with boninite. These dykes were interpreted by Brown (1986) to represent feeders for the boninitic lavas.

Volcanic rocks

Low-Ti tholeiitic basalt occurs as massive and pillowed aphyric flows that commonly exhibit a regular variation in grain size normal to flow contacts. They display amygdaloidal, variolitic, ophitic,

TABLE 1(a). MEAN PRECIOUS METAL AND TRACE ELEMENT CONCENTRATIONS OF THE CUMALTE ROCKS IN THE HEAZLEWOOD RIVER COMPLEX

| TYPE | | Os | Ir | Ru | Pt | Rh | Au | Ni | Cu | S | Mg # | Pt/Ir | Pt/Pd |
|-------|-------|-------------|--------------|-------------|-----------|-------------|--------------|-----------|-----------|-----------|------------|-----------|-----------|
| DUN | n | 8 | 44 | 44 | 44 | 35 | 44 | 49 | 44 | 32 | 49 | 44 | 44 |
| | mean | 7.94±10.8 | 0.616±1.11 | 3.24±2.17 | 2.88±23.4 | 0.631±0.480 | 0.126±0.082 | 2130±458 | 6.97±61.5 | 47.3±35.7 | 89.6±3.20 | 4.47±64.9 | 5.13±19.0 |
| | range | 2.1-34.0 | 0.02-5.09 | 0.6-9.5 | 0.2-120 | <0.2-2.5 | 0.02-0.31 | 1170-2960 | <1-408 | <20-184 | 82.8-94.0 | 0.06-353 | 0.22-105 |
| HAR | n | 3 | 23 | 23 | 23 | 20 | 23 | 23 | 20 | 22 | 23 | 23 | 20 |
| | mean | 0.630±0.609 | 0.265±0.201 | 1.97±1.44 | 8.69±6.28 | 0.910±2.12 | 0.096±0.078 | 1400±325 | 12.1±37.1 | 65.6±74.2 | 86.7±2.07 | 32.7±25.9 | 10.8±17.5 |
| | range | 0.2-1.4 | 0.04-0.89 | 0.5-5.3 | 1.2-21.2 | <0.3-9.9 | 0.02-0.30 | 967-2250 | <1-120 | <20-384 | 83.0-91.1 | 5.45-98.6 | 2.09-74.3 |
| PL-PD | n | - | 7 | 7 | 7 | 7 | 7 | 8 | 8 | 8 | 8 | 7 | 7 |
| | mean | - | 0.165±0.130 | 1.12±0.945 | 6.02±2.64 | 5.07±3.86 | 0.302±0.206 | 914±368 | 33.6±26.1 | 83.0±99.2 | 82.8±4.27 | 36.5±73.4 | 1.19±1.77 |
| | range | - | 0.05-0.34 | 0.7-3.4 | 2.8-10.5 | 0.5-10.8 | 0.16-0.77 | 212-1300 | 11-80 | <20-277 | 72.7-86.2 | 8.81-210 | 0.61-5.53 |
| WEHR | n | - | 10 | 10 | 8 | 8 | 8 | 10 | 10 | 4 | 10 | 10 | 8 |
| | mean | - | 0.172±0.0900 | 1.54±0.729 | 31.2±12.7 | 0.982±0.689 | 0.195±0.147 | 759±124 | 27.2±39.4 | 34.9±22.9 | 85.5±2.08 | 182±160 | 29.6±8.47 |
| | range | - | 0.05-0.33 | 0.6-2.9 | 19.1-53.2 | 0.4-2.6 | 0.11-0.50 | 514-910 | 13-144 | <20-70 | 81.7-88.5 | 83.0-537 | 19.2-45.5 |
| OPX | n | 12 | 39 | 37 | 39 | 26 | 39 | 43 | 39 | 26 | 43 | 39 | 26 |
| | mean | 0.701±0.804 | 0.148±0.131 | 1.41±1.01 | 6.17±19.1 | 0.598±0.918 | 0.0791±0.182 | 717±206 | 6.19±42.7 | 44.4±58.1 | 86.2±2.74 | 41.7±183 | 14.5±34.3 |
| | range | 0.02-2.8 | 0.01-0.37 | <0.4-4.2 | 0.3-78.9 | <0.2-2.9 | 0.03-0.96 | 368-1200 | <1-271 | <20-268 | 81.3-93.1 | 2.00-1050 | 1.52-136 |
| TROC | n | 3 | - | 6 | 8 | 8 | 8 | 8 | 6 | 7 | 8 | 8 | 8 |
| | mean | 0.931±0.987 | 0.316±0.311 | 2.95±0.954 | 4.27±2.71 | 1.56±0.548 | 0.0912±0.070 | 1120±261 | 12.1±7.31 | 83.2±84.0 | 86.5±0.989 | 13.5±15.1 | 2.74±1.48 |
| | range | 0.5-2.3 | 0.09-1.09 | <0.3-4.6 | 2.6-9.7 | 0.9-2.5 | 0.03-0.21 | 850-1650 | <1-23 | <20-271 | 85.3-88.2 | 6.67-48.5 | 1.12-6.06 |
| PL-PX | n | - | 8 | 8 | 9 | 9 | 9 | 13 | 13 | 7 | 13 | 8 | 9 |
| | mean | - | 0.0571±0.060 | 0.787±0.836 | 3.99±3.72 | 1.91±3.90 | 0.145±0.593 | 485±209 | 10.7±7.21 | 47.4±9.43 | 82.2±3.74 | 88.5±203 | 2.09±3.82 |
| | range | - | <0.01-0.17 | <0.4-2.3 | 0.6-11.0 | 0.4-12.9 | 0.5-1.89 | 284-1040 | 4-26 | <20-61 | 77.1-89.7 | 22.0-620 | 0.48-12.1 |

Notes: Average values represent geometric means for the PGE, Pt/Ir and Pt/Ru and arithmetic means for trace elements and Mg#. Mg# = 100Mg/(Mg+Fe²⁺) where total iron is reported as FeO. Platinum-group element data are in ppb. Nickel, Cu and S data are in ppm. Standard deviation based on N-1 (1 sigma). N=number of samples above the detection limit, from which the mean and standard deviation were calculated. Abbreviations: DUN-dunite; HAR-harzburgit; PL-PD-plagioclase peridotite; WEHR-wehrilit; OPX-orthopyroxenite; TROC-troctolite; PL-PX-plagioclase pyroxenite.

TABLE 1(b). DYKES AND VOLCANIC ROCKS

| TYPE | | Os | Ir | Ru | Pt | Rh | Au | Ni | Cu | S | Mg # | Pt/Ir | Pt/Pd |
|------|-------|-------------|---------------|-------------|-----------|-----------|-------------|-----------|-----------|-----------|-----------|-----------|-------------|
| FGG | n | - | 10 | 8 | 10 | 9 | 10 | 20 | 20 | 11 | 20 | 10 | 9 |
| | mean | - | 0.0428±0.034 | 0.561±0.497 | 9.35±16.9 | 12.4±10.9 | 0.396±4.96 | 235±168 | 19.9±275 | 116±954 | 70.1±11.7 | 218±226 | 0.613±0.632 |
| | range | - | 0.01-0.10 | <0.2-1.8 | 2.8-60.7 | <0.4-36.0 | 0.13-16.0 | 34-566 | 2-1250 | <20-3260 | 40.5-86.9 | 66.0-607 | 0.26-1.94 |
| ANOR | n | - | 2 | 2 | 2 | 2 | 2 | 5 | 5 | 3 | 5 | 2 | 2 |
| | mean | - | 0.0412 | 0.374 | 7.67 | 3.81 | 1.66 | 71.2±30.6 | 35.3±118 | 71.1±85.1 | 62.0±19.6 | 186 | 2.01 |
| | range | - | - | - | - | - | - | 30-104 | 6-287 | <20-191 | 36.9-85.2 | - | - |
| CGG | n | 1 | 8 | 8 | 9 | 9 | 9 | 18 | 18 | 6 | 18 | 8 | 9 |
| | mean | 0.1 | 0.0172±0.031 | 0.229±0.266 | 3.31±4.73 | 2.18±7.61 | 0.103±0.248 | 259±106 | 13.1±7.02 | 41.9±23.1 | 78.6±6.95 | 195±906 | 1.52±2.25 |
| | range | - | 0.003-0.09 | 0.1-0.7 | 0.8-14.6 | 0.2-25.1 | 0.03-0.86 | 100-461 | 2-30 | <20-94 | 59.2-85.0 | 11.1-2880 | 0.20-6.50 |
| BAPX | n | - | 2 | 2 | 2 | 2 | 2 | 3 | 3 | - | 3 | 2 | 2 |
| | mean | - | 0.0300 | 1.37 | 8.72 | 5.59 | 0.594 | 540±28.8 | 14.5±6.66 | - | 80.6±3.85 | 291 | 1.56 |
| | range | - | - | - | - | - | - | 509-566 | 11-23 | - | 76.6-84.3 | - | - |
| LOTI | n | 3 | 9 | 5 | 9 | 9 | 9 | 20 | 20 | 18 | 20 | 9 | 9 |
| | mean | 0.638±0.493 | 0.0888±0.068 | 1.12±0.758 | 12.4±7.23 | 15.7±5.96 | 0.981±1.49 | 92.6±28.5 | 82.8±95.2 | 173±219 | 61.7±3.93 | 140±355 | 0.790±0.369 |
| | range | 0.4-1.3 | 0.01-0.21 | <0.5-2.4 | 8.0-32.0 | 10.4-30.6 | 0.4-5.20 | 54-175 | 15-464 | <20-760 | 55.3-68.1 | 47.1-1150 | 0.38-1.61 |
| BON | n | - | 6 | 6 | 6 | 6 | 6 | 6 | 6 | 5 | 6 | 6 | 6 |
| | mean | - | 0.0705±0.0308 | 1.18±0.250 | 5.44±4.41 | 5.45±1.91 | 0.437±0.864 | 522±137 | 27.0±150 | 24.6±5.37 | 78.0±3.46 | 77.1±51.5 | 0.998±1.17 |
| | range | - | 0.05-0.13 | 0.9-1.6 | 2.3-14.1 | 3.7-8.1 | 0.16-2.37 | 359-728 | 6-387 | <20-31 | 72.9-82.6 | 38.3-182 | 0.44-3.62 |

Abbreviations: FGG-fine-grained gabbro-norite dykes; ANOR-anorthosite dykes; CGG-coarse-grained gabbro-norite dykes; BAPX-basaltic pyroxenite dykes; LOTI-low-Ti tholeiitic basalt; BON-boninite.

TABLE 2. WEIGHTED MEAN PRECIOUS METAL AND TRACE ELEMENT CONCENTRATIONS OF THE MAJOR CUMULATE SEQUENCES IN THE HEAZLEWOOD RIVER COMPLEX

| UNIT | Os | Ir | Ru | Pt | Rh | Au | Ni | Cu | S | Mg# | PdIr | PtPd |
|--------|---------------|-----------------------------|--------------------------------|-----------------------------|-----------------------------|-------------------------------|----------------------------|--------------------------|---------------------------|-----------------------------|----------------------------|-----------------------------|
| NM | mean range | 0.68±1.25 (32) 0.01-5.09 | 3.43±2.17 (31) <0.4-9.5 | 1.99±3.34 (32) 0.2-14.9 | 0.55±0.378 (22) 0.1-1.3 | 0.13±0.0790 (32) 0.02-0.44 | 21.40±271 (32) 737-2960 | 6.40±14.1 (30) <1-78 | 42.1±16.2 (15) <20-105 | 91.1±1.47 (32) 83.7-94.0 | 7.57±56.9 (32) 0.06-385 | 4.31±6.39 (22) 0.22-85.0 |
| FS(dn) | mean range | 2.8 (1) - | 1.81 (4) 1.1-2.7 | 14.0 (4) 2.0-78.9 | 0.633 (4) 0.4-1.7 | 0.192 (4) 0.10-0.31 | 1620±148 (5) 557-2110 | 49±227 (5) 3-408 | 38.3 (3) <20-45 | 87.5±0.71 (5) 85.2-88.7 | 51.2 (4) 1.21-359 | 16.7 (5) 2.83-46.4 |
| FS(gx) | mean range | 1.18±0.57 (5) 0.9-2.1 | 0.25±0.104 (30) 0.6-4.2 | 1.66±0.821 (30) 0.3-1.20 | 0.63±0.395 (21) <0.2-2.6 | 0.18±0.110 (28) 0.03-0.56 | 1000±164 (31) 387-1740 | 25.6±48.8 (29) <1-271 | 38.7±21.8 (17) <20-109 | 85.5±1.63 (31) 81.7-88.5 | 78.8±9.6 (30) 2.00-337 | 44.4±26.1 (21) 9.67-136 |
| GH(gx) | mean range | 0.4 (1) - | 0.18±0.020 (8) 0.15-0.22 | 1.56±0.568 (8) 0.9-2.6 | 2.64±1.78 (8) 0.7-9.2 | 0.430±0.967 (5) <0.3-2.2 | 1040±238 (8) 631-2060 | 4.26±12.5 (8) 1-31 | 51.5±8.08 (8) <20-184 | 85.8±3.18 (8) 82.8-90.4 | 13.1±9.04 (8) 4.67-61.3 | 9.42±15.5 (5) 2.36-36.0 |
| CH(w) | mean range | - - | 0.128±0.0316 (6) 0.09-0.17 | 1.20±1.12 (5) <0.6-3.4 | 5.10±1.78 (6) 3.4-9.7 | 0.974±0.608 (6) 0.2-3.0 | 619±171 (12) 280-1040 | 10.6±8.86 (12) 1-27 | 49.3±13.5 (7) <20-74 | 81.5±1.59 (12) 77.1-85.1 | 40.0±20.1 (6) 20.0-80.8 | 8.80±5.49 (6) 1.87-20.5 |
| GH(dn) | mean range | - - | 0.195±0.0670 (8) 0.11-0.39 | 1.67±0.769 (8) 0.9-3.5 | 5.61±6.67 (8) 0.9-21.0 | 1.13 (3) <0.3-2.2 | 1140±197 (8) 484-1590 | 3.79±1.73 (7) <1-1 | 46.9±14.1 (8) 34-81 | 87.4±2.78 (8) 83.0-93.1 | 33.3±32.1 (8) 4.29-100 | 8.79 (3) 5.36-12.0 |
| GH(gx) | mean range | - - | 0.028±0.0316 (6) <0.01-0.10 | 0.740±0.667 (7) 0.1-1.6 | 3.93±4.44 (7) 0.6-11.0 | 1.61±0.85 (6) 0.4-12.9 | 422±94.2 (7) 168-536 | 7.25±5.45 (7) 1-15 | 39.3±11.3 (5) <20-61 | 84.0±2.44 (7) 80.9-88.1 | 21.7±6.07 (6) 37.1-1050 | 2.05±1.73 (6) 0.85-4.50 |
| PP(dn) | mean range | 2.1 (1) - | 0.464 (4) 0.20-0.61 | 1.47 (4) 1.2-2.8 | 8.87 (4) 2.7-17.9 | 0.810 (4) 0.2-2.1 | 1530 (4) 1010-1920 | 24.9 (4) <1-20 | 76.1 (4) <20-91 | 85.7 (4) 83.3-87.4 | 23.2 (4) 4.49-79.3 | 9.94 (4) 6.63-16.9 |
| PP(1) | mean range | 0.592 (2) 0.5-0.7 | 0.49±0.245 (14) 0.04-1.56 | 2.49±0.983 (13) <1.0-4.6 | 3.44±1.04 (14) 1.1-11.4 | 0.135±0.0751 (14) 0.4-10.3 | 1320±315 (14) 562-2100 | 19.1±16.9 (12) <1-77 | 69.9±24.1 (13) <20-104 | 86.1±1.22 (14) 83.2-88.6 | 21.5±33.6 (14) 2.12-210 | 3.13±2.17 (14) 0.73-13.1 |
| BH | mean range | 0.949 (4) 0.2-2.3 | 0.34±0.251 (30) 0.03-1.15 | 2.90±1.22 (28) <0.3-7.2 | 7.85±5.99 (30) 2.2-42.6 | 1.32±1.56 (30) 0.1-10.1 | 1370±386 (34) 34-2330 | 14.8±9.48 (30) <1-80 | 121±81.9 (28) <20-384 | 87.3±2.47 (34) 82.0-94.2 | 31.9±26.8 (30) 4.52-213 | 7.09±12.2 (30) 0.48-74.3 |

Mean values were calculated using the weighting factors and averages in Appendix 1. Standard deviation represents the weighted mean of the deviations reported in Appendix 1. Values in brackets above the detection limit, which were used in the calculation of the mean. Platinum-group element data are in ppb. Trace elements are in ppm. Mg# = 100(Mg/Mg+Fe²⁺), where total Fe is reported as FeO. Abbreviations for units: NM-19 Mile Creek dunite sequence; FS(dn), Fenton's Spar dunite sequence; FS(gx), Fenton's Spar pyroxenite sequence; CH(w)-Caudry's Hill orthopyroxenite sequence; CH(gx)-Caudry's Hill plagioclase websterite sequence; GH(dn)-Gabbro Hill dunite sequence; GH(gx)-Gabbro Hill plagioclase pyroxenite sequence; PP(dn)-Purcell's Plain dunite sequence; PP(1)-Purcell's Plain ilmenite sequence; BH-Brassay Hill harzburgite sequence.

subophitic and granophyric textures. They locally contain primary plagioclase–augite assemblages with accessory magnetite and Fe–Ti spinel, but are more commonly metamorphosed at the prehnite–pumpellyite and greenschist facies (Creanaune 1980, this study). The basaltic rocks vary from quartz-normative to olivine-normative in composition (Creanaune 1980). Boninite lavas in the HRC are poorly exposed and deeply weathered. They commonly display porphyritic, glomeroporphyritic and vesicular textures, and some lavas display flow-banding (Brown 1986). The primary mineralogy of the boninite is believed to have consisted of orthopyroxene and clinoenstatite phenocrysts set in a finer-grained groundmass of pyroxene, plagioclase and accessory Cr-spinel (Brown 1986). Limited field evidence presented by Brown (1986) indicates that the low-Ti tholeiite lavas are younger than the boninitic lavas.

Tonalite complex

Creanaune (1980) described the tonalite complex in the northeastern part of the HRC (Fig. 2) as comprising trondhjemite, diorite, dolerite and tonalite, which represent, in his opinion, highly differentiated end-members that belong to the ultramafic series. Tonalitic rocks outcrop as smaller dykes in other parts of the complex and include plagiogranite that intrudes the Brassey Hill harzburgite sequence. Mapping by the present authors demonstrated that gabbroic rocks and ultramafic xenoliths also are abundant within the tonalite complex. The tonalite suite is interpreted to represent the youngest component of the HRC and has a U–Pb (zircon) age of 520 Ma (Brown 1986).

GEOCHEMISTRY

Analytical methods

Grab samples from surface outcrops were analyzed for major and trace elements using an ARL 8420 X-ray fluorescence spectrometer following the procedure described by Haukka & Thomas (1977). Precious metals and Se were determined by radiochemical neutron-activation analysis (RNAA) using the fire-assay preconcentration method outlined by Hoatson & Keays (1990). All analyses were carried out at the Department of Geology, University of Melbourne. Analytical precision, based on replicate analyses of international and in-house rock standards, is as follows: trace elements $< \pm 10\%$; *PGE* and Au $< \pm 15\%$; Se $< \pm 20\%$.

The mean whole-rock abundances of the *PGE*, Au, Ni, Cu and S, and the average values for Mg#, Pt/Ir and Pt/Pd for the major rock types occurring in the Heazlewood River complex are listed in Table

1. The weighted mean abundances of these parameters for the major sequences of cumulates are listed in Table 2, and are based on the data given in Appendix 1. Geometric means are used for the precious metals, Cu and S because they display log-normal distributions. The data were derived from 230 individual whole-rock analyses, including 158 ultramafic cumulates, 46 dykes and 26 volcanic rocks. Nickel and Mg# are used as fractionation indices, as they exhibit strong correlations with abundances of incompatible elements in the dykes and volcanic rocks (which are considered to approximate liquid compositions). Copper and S data are presented so that the relationships between the precious metals and chalcophile elements can be examined. The Pt/Ir ratio is an indicator of the degree of (Os + Ir + Ru):(Pt + Pd + Rh) fractionation, and is used in preference to Pd/Ir because Pd concentrations were not obtained for all of the samples. The Pt/Pd value is listed because it is known to reflect the genetic and tectonic association of ultramafic intrusions (Naldrett & Cabri 1976). Despite the strong association between *PGE* and chromite in ultramafic rocks (e.g., Agiorgitis *et al.* 1977), Cr data are omitted because the interpretation of Cr abundances is complicated by the fact that it is a major element in spinel and a trace element in pyroxene. Samples were screened for weathering and alteration (excluding serpentinization). The use of serpentinized rocks was unavoidable in many areas, but the *PGE* are believed to be relatively immobile during serpentinization (e.g., Oshin & Crockett 1982). The volcanic rocks record low-grade metamorphism, which also appears to have had little effect on the primary abundances of the *PGE* (Barnes *et al.* 1985). The presence of Au-, Pt- and Pd-enriched Ni-sulfide occurrences in shear zones and faults that cut the cumulate sequences (Mann 1988) indicates that these elements were mobile under certain conditions.

S and Se in the Heazlewood River Complex

Before a discussion of the abundances of the precious metals, it is important to establish the fact that the complex was derived from S-poor magmas. The S content of the parental liquids for the cumulates can be estimated from the S abundances of the ultramafic rocks. Over 90% of the cumulates contain < 100 ppm S. The highest average tenor of S is displayed by the plagioclase-bearing cumulates, but these values also are < 100 ppm (Table 1). The plagioclase-bearing cumulates commonly contain 25% or more postcumulus minerals, which reflects the proportion of trapped intercumulus liquid or cumulate porosity. If we assume that the tenor of S in the intercumulus liquids was equivalent to that of the parental magmas (*i.e.*, S behaved as an incompatible element and crystallization had not

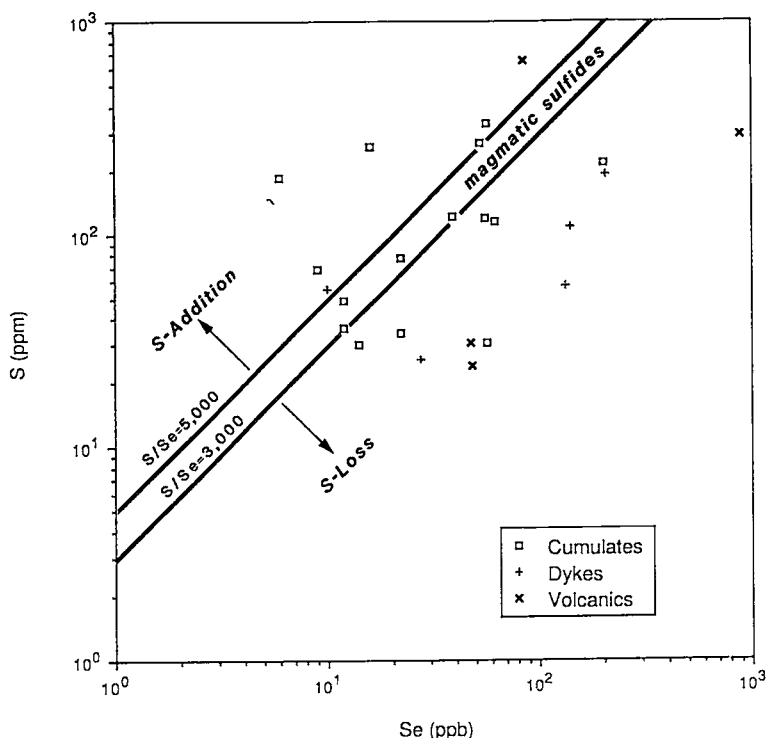


FIG. 3. S/Se plot for selected rock types from the Heazlewood River complex.

progressed beyond 90%), and that the average tenor of S in the rocks was < 100 ppm, then the maximum S content of the parental magmas was < 400 ppm. An additional estimate of the S content of the parental magmas is given by the volcanic rocks that are considered to be genetically related to the cumulates (e.g., Brown 1986). The boninites display S abundances of < 100 ppm, and over 80% of the low-Ti basalts have S contents below 300 ppm. All of these estimates are considerably lower than the levels at which magmatic sulfides would be expected to form (500–2,000 ppm; Haughton *et al.* 1974). This observation is supported by the absence of cumulus sulfides in any of the samples examined from the ultramafic sequences. Small amounts of sulfides (pyrite, pyrrhotite, chalcopyrite) are locally observed in the volcanic rocks, but these appear to be hydrothermal in origin, as they occur with quartz as amygdale- and fracture-fillings or as massive replacement bodies in brecciated basalt. Heazlewoodite is locally observed in serpentinites developed in shear zones and faults, but is clearly the product of serpentinizing fluids (e.g., Eckstrand 1975).

A limited number of data on Se were obtained and are presented on a Se *versus* S plot (Fig. 3). The S/Se values for most of the samples fall outside of the field for igneous rocks, which reflects the greater mobil-

ity of S relative to Se (Howard 1977) during low-temperature alteration. The S/Se data indicate that both S addition and S loss occurred during the alteration of the complex. The presence of heazlewoodite in many of the serpentinized cumulates is believed to be a reflection of subsolidus addition of S that occurred during serpentinization of the rocks. The replacement of precious-metal and base-metal sulfides by alloys was observed in altered chromitites from the HRC (Peck & Keays 1990), and is testimony to the local removal of S during subsolidus alteration of the cumulates.

The low mean abundances of S in the dykes and volcanic rocks (< 20 to 173 ppm) documented here are comparable to the data given by Hamlyn *et al.* (1985) for boninites and low-Ti lavas (< 20–457 ppm, mean < 54 ppm). These primitive lavas are believed to represent second-stage melts derived from depleted mantle (Hamlyn & Keays 1986). They do not contain primary sulfides and constitute excellent examples of S-undersaturated liquids.

In summary, the low tenor of S in mafic and ultramafic rocks from the Heazlewood River complex indicates that it was derived from S-undersaturated magmas; consequently, the distribution of precious metals was not influenced by the development of cumulus sulfides.

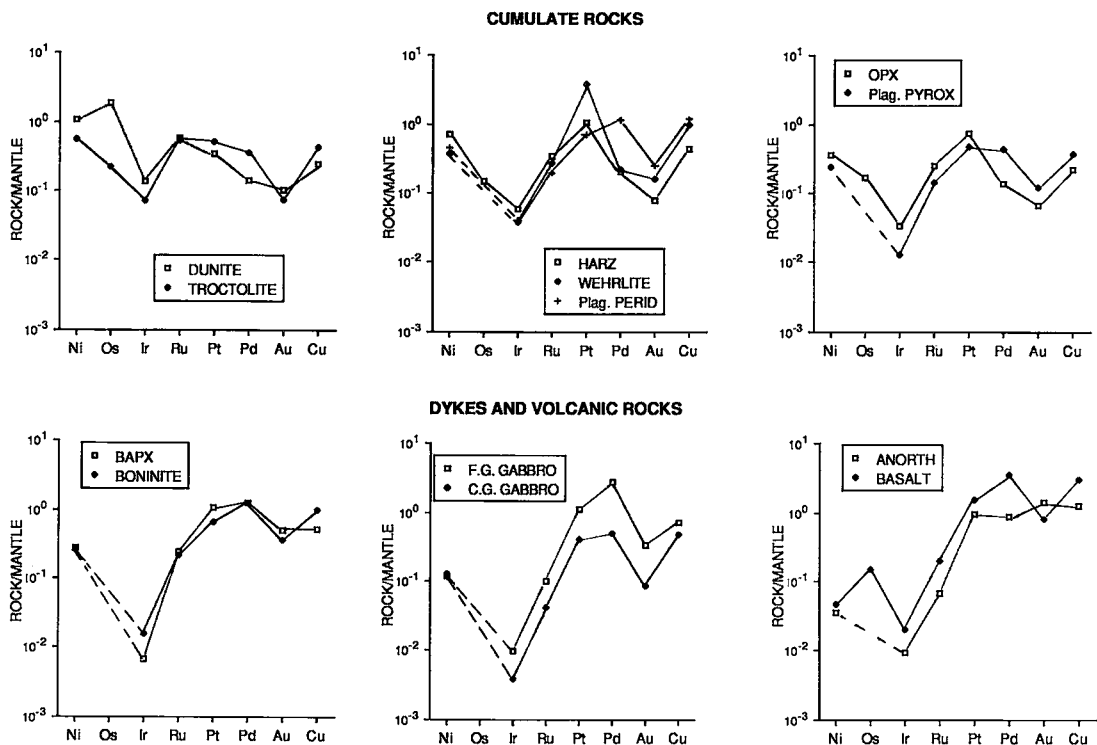


FIG. 4. Mantle-normalized metal abundances (Barnes *et al.* 1988) for the major rock types in the Heazlewood River complex. The raw data are derived from Table 1. Mantle values, given by Barnes *et al.* (1985), are as follows: 2000 ppm Ni, 4.2 ppb Os, 4.4 ppb Ir, 6 ppb Ru, 2 ppb Rh, 9.2 ppb Pt, 4.4 ppb Pd, 1.4 ppb Au, and 28 ppm Cu. Abbreviations: HARZ harzburgite, Plag. PERID plagioclase peridotite, OPX orthopyroxenite, Plag. PYROX plagioclase orthopyroxenite and plagioclase websterite, F.G. GABBRO fine-grained gabbronorite dykes, C.G. GABBRO coarse-grained gabbronorite dykes, BAPX basaltic pyroxenite dykes, ANORTH anorthositic dykes, BASALT low-Ti tholeiitic basalt.

Distribution of precious metals in the Heazlewood River Complex

The absolute abundances of the *PGE* and Au are quite low for all of the major cumulate rock types (Table 1). Total *PGE* abundances are highest in wehrlite (34 ppb) and lowest in plagioclase pyroxenite and orthopyroxenite (6.7 and 9.0 ppb, respectively). Of the noncumulate rocks, low-Ti basalt (30 ppb) and fine-grained gabbronorite (22 ppb) have the highest abundance of total *PGE*, and coarse-grained gabbronorite (5.8 ppb), the lowest.

As the order of primary crystallization recorded in the cumulate rocks of the HRC is olivine → orthopyroxene → clinopyroxene (where present), and given the nature of cyclic units in the Brassey Hill sequence, it is possible to construct an idealized succession of cumulates for the complex. The most primitive rocks are dunite or plagioclase-bearing dunite. Peridotite samples represent an intermediate composition. The most evolved cumulates are

orthopyroxenite and plagioclase pyroxenite. Plots of mantle-normalized abundances (Barnes *et al.* 1988) provide a useful means of examining the variations in *PGE* abundances through this idealized succession. Such plots for the HRC (Fig. 4) reveal that dunite and troctolite display negatively sloping and flat patterns, respectively, which highlights their relative enrichment in Ni and *IPGE* (the iridium group of the *PGE*; cf. Barnes *et al.* 1985). In contrast, samples of the more evolved pyroxenite display positively sloping patterns from Ir to Pt (Fig. 4), which reflects a relative enrichment in *PPGE* (the palladium group of the *PGE*). Peridotite samples display similar patterns to those of the pyroxenite, but have higher relative Ni and Ir abundances, a reflection of their more primitive composition. Both the dykes and the volcanic rocks display pronounced positively sloping patterns from Ir to Pd, as is typical of mafic magmas in general (Barnes *et al.* 1988). They contain much higher average *PPGE* and Cu and much lower *IPGE* concentrations than the cumulates. These patterns

indicate that the *PPGE* and Cu were preferentially incorporated into residual liquid, and the *IPGE* and Ni were strongly partitioned into the most primitive cumulates during the formation of the HRC.

Several anomalous patterns can be identified on the abundance plots (Fig. 4), for example negative Ir anomalies for most of the rock types, negative Pd and Au anomalies for the cumulates, and positive Pt anomalies for the peridotites. The significance of these features will be considered in a later section.

The observed enrichment in *IPGE* in the early-formed olivine-rich cumulates reflects the decoupling of Os, Ir and Ru from the *PPGE*, as has been documented in several recent studies (e.g., Agiorgitis *et al.* 1977, Oshin & Crocket 1982, Page & Talkington 1984). This decoupling can be gauged by examining the variations in the mean Pt/Ir value for the cumulates (Table 1). The Pt/Ir ratio increases from the most primitive cumulates (dunite and troctolite) through harzburgite and plagioclase peridotite, to the most evolved cumulates (orthopyroxenite and plagioclase pyroxenite). This trend extends to the dykes and volcanic suites, which display lower Mg# and generally higher Pt/Ir than the cumulates (Table 1). The unusually high mean Pt/Ir value for wehrlite (182) reflects the anomalously high Pt abundances in the cumulate rocks from a single locality (Fenton's Spur), as will be discussed below.

Evolutionary trends involving the precious metals are most pronounced in dunite, in which Pt shows a negative correlation with the Ni/Co fractionation index, and Ir displays a positive covariation with Ni/Co (Fig. 5). A positive correlation exists between Ir and Ru in the dunites (Fig. 5, Table 3), but is much less significant in the volcanic rocks (Table 4).

Correlation matrices for the dunites and the volcanic rocks (Tables 3, 4) show that the precious metals have few geochemical analogues amongst the major and trace elements. Some of the dispersion in the data may reflect variations in the absolute abundances of the elements from one locality to the next, as well as differences in porosity of the cumulate rocks. Nickel displays a weak positive correlation with the *IPGE* in dunite, and Pd behaves sym-

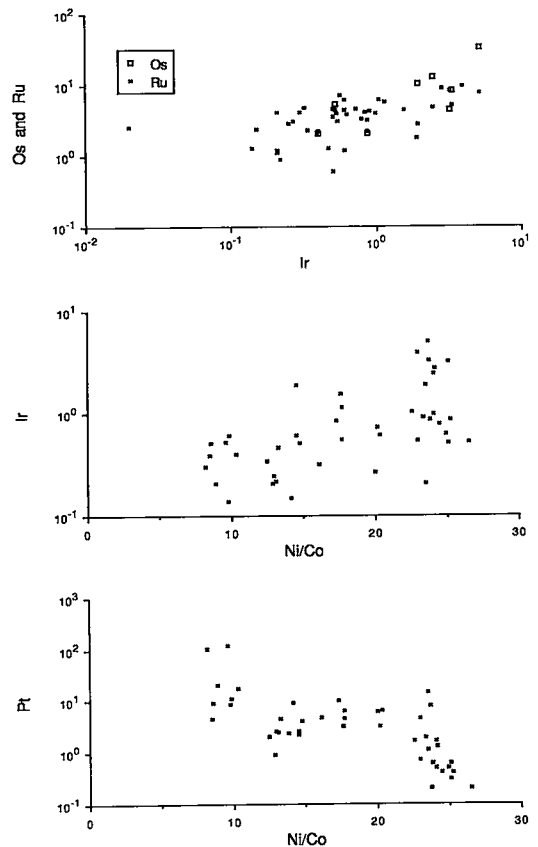


FIG. 5. Selected binary plots for dunites from the Heazlewood River complex. Based on unpublished whole-rock data (Peck & Keays).

pathetically with Al and Fe^{3+} and antipathetically with Cr, Ni and Mg in the volcanic rocks. Palladium, Pt and Au display weak to moderate positive correlation in the volcanic rocks and, to a lesser degree, in the cumulates (Tables 3, 4). Palladium and Au abundances are extremely low and display little variation in the cumulates. Their abundance appears to

TABLE 3. CORRELATION MATRIX FOR DUNITES

| | Os | Ir | Ru | Pt | Pd | Au | Cr | Ni | Cu | S | MgO | Fe2O3 | Al2O3 | LOSS | |
|-------|--------|--------|--------|--------|---------|--------|--------|--------|--------|-------|--------|-------|--------|--------|------|
| Os | ++++ | 0.811 | 0.573 | 0.487 | no data | 0.307 | 0.520 | 0.360 | 0.172 | | 0.347 | 0.432 | 0.540 | 0.360 | |
| Ir | | ++++ | 0.673 | | 0.135 | | 0.471 | 0.471 | 0.100 | | 0.263 | | 0.066 | 0.381 | |
| Ru | | | ++++ | | 0.400 | | 0.076 | 0.488 | | | 0.339 | | | 0.452 | |
| Pt | | -0.129 | -0.003 | ++++ | 0.500 | 0.283 | | | 0.034 | 0.074 | | 0.462 | | | |
| Pd | | | | | ++++ | 0.377 | | | | 0.105 | | 0.270 | 0.125 | 0.386 | |
| Au | | -0.073 | -0.019 | | | ++++ | | | 0.150 | | | 0.371 | | | |
| Cr | | -0.329 | | | | | ++++ | | | 0.293 | | 0.288 | 0.391 | | |
| Ni | | | | -0.338 | -0.087 | -0.247 | | ++++ | | | 0.695 | | | 0.503 | |
| Cu | | | -0.164 | -0.025 | -0.117 | -0.225 | -0.051 | -0.003 | ++++ | | 0.032 | 0.179 | | | |
| S | -0.024 | -0.167 | -0.074 | | -0.311 | -0.094 | -0.301 | -0.094 | ++++ | ++++ | 0.262 | 0.308 | | | |
| MgO | | | | -0.086 | -0.120 | -0.117 | -0.225 | -0.094 | -0.445 | ++++ | ++++ | 0.336 | | 0.307 | |
| Fe2O3 | | -0.259 | -0.183 | | | | -0.774 | -0.738 | | | ++++ | ++++ | | | |
| Al2O3 | | -0.009 | | -0.034 | -0.066 | | -0.129 | -0.019 | | | -0.468 | ++++ | | | |
| LOSS | | | | -0.224 | -0.018 | -0.387 | | -0.285 | -0.145 | | | | -0.681 | -0.141 | ++++ |

Notes: All variables represent unnormalized whole-rock abundances. Fe2O3=total iron. LOSS=Loss on ignition.

TABLE 4. CORRELATION MATRIX FOR LOW-TI THOLEIITIC BASALTS AND BONINITES

| | Ir | Ru | Pt | Pd | Au | Cr | Ni | Cu | S | MgO | Fe2O3 | Al2O3 | LOSS |
|-------|--------|--------|--------|--------|--------|--------|--------|--------|--------|--------|--------|-------|-------|
| Ir | ++++ | | 0.199 | 0.065 | 0.021 | | | 0.170 | 0.012 | | | 0.311 | |
| Ru | -0.137 | ++++ | | 0.065 | | 0.303 | 0.356 | | 0.313 | 0.284 | 0.453 | | 0.117 |
| Pt | -0.265 | -0.265 | ++++ | 0.496 | 0.776 | | | 0.449 | 0.084 | | 0.450 | 0.368 | |
| Pd | -0.124 | | | ++++ | 0.332 | | | | 0.499 | | 0.700 | 0.675 | |
| Au | | -0.248 | | | ++++ | | | 0.101 | 0.037 | | 0.307 | 0.218 | |
| Cr | -0.234 | | -0.435 | -0.714 | -0.135 | ++++ | 0.967 | | | 0.963 | | | 0.631 |
| Ni | -0.326 | | -0.505 | -0.675 | -0.126 | | ++++ | | | 0.902 | | | 0.659 |
| Cu | | -0.255 | | -0.066 | | -0.054 | -0.174 | ++++ | 0.225 | 0.046 | 0.349 | | |
| S | | | | | | -0.445 | -0.411 | | ++++ | | 0.354 | 0.413 | |
| MgO | -0.139 | | -0.370 | -0.740 | -0.201 | | | | -0.447 | ++++ | | | |
| Fe2O3 | -0.082 | | | | | -0.196 | -0.137 | | | -0.203 | ++++ | 0.091 | |
| Al2O3 | | -0.428 | | | | -0.939 | -0.915 | | -0.022 | -0.933 | | ++++ | 0.655 |
| Loss | -0.386 | | -0.531 | -0.596 | -0.252 | | | -0.067 | -0.327 | -0.295 | -0.655 | | ++++ |

Notes: All variables represent unnormalized whole-rock abundances. Fe2O3=total iron. LOSS=Loss on ignition.

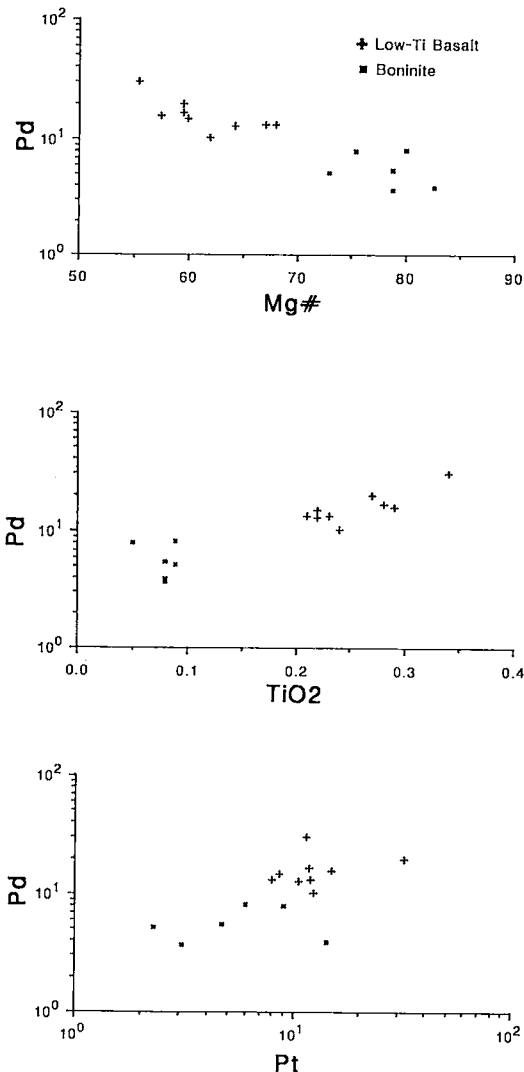


FIG. 6. Selected binary plots for volcanic rocks from the Heazlewood River complex. Based on unpublished whole-rock data (Peck & Keays).

be strongly influenced by cumulate porosity, with the more porous plagioclase-bearing rocks having higher concentrations (Table 1). The fact that Pd and Au abundances are much higher in the non-cumulate rocks supports this contention. Platinum is selectively enriched in peridotite and, in particular, wehrlite (mean 31.2 ppb), within the cumulate sequences. It otherwise exhibits a distribution similar to that of Pd and Au, being concentrated in the most evolved rocks (low-Ti basalt; mean 12.4 ppb Pt). A plot of Pt versus Pd concentrations for the volcanic rocks shows that a moderate positive correlation exists between the two metals (Fig. 6). The incompatible behavior of Pd in the volcanic suites is illustrated by its sympathetic behavior with Ti and strong negative correlation with whole-rock Mg# (Fig. 6).

The low-Ti basalt and boninite suites of the HRC are considered to be the most likely candidates for parental liquids for the cumulate sequences, although the details of this association are still being investigated. Given this assumption, an index of compatibility (CI) for a given element in the early stages of fractional crystallization can be obtained from the ratio of the concentration of the element in the parental liquid (C_L , approximated by the mean values for basalt or boninite given in Table 1b) to its concentration in early-formed solid phases (C_S , here taken as the dunite cumulates, see Table 1a). Therefore, $CI = C_S / (C_S + C_L)$. This is similar to the equation for the elemental distribution coefficient, K_d , where $K_d = C_S / C_L$, but differs in that two mineral phases occur in dunite (olivine and chromite), and CI is restricted to values between 0 and 1, with higher values representing greater degrees of compatibility. Using the low-Ti tholeiitic basalt - dunite combination, the following CI values are obtained: Os (0.93) > Ir (0.87) > Ru (0.74) > Pt (0.19) > Au (0.11) > Pd (0.04). If boninite is substituted, then the sequence is: Ir (0.90) > Ru (0.73) > Pt (0.35) > Au (0.22) > Pd (0.10). Therefore, the PGE are partitioned into early-formed cumulates in order of their melting points, with Au having a compatibility intermediate between that of Pt and Pd.

An overview of these relationships is given in

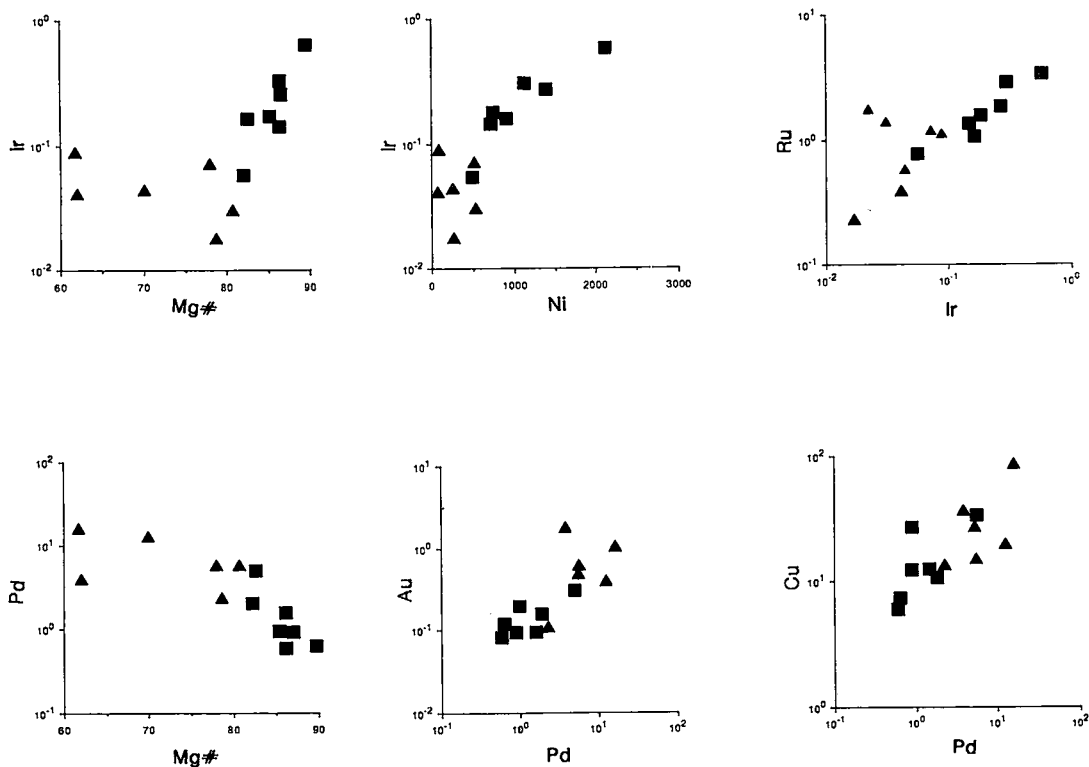


Fig. 7. Selected binary plots based on mean values of abundances of precious metal and trace elements and whole-rock Mg# for the major rock types in the Heazlewood River complex (data are given in Table 1). Symbols: squares: cumulates, triangles: dykes and volcanic rocks.

Figure 7, in which the mean abundance data from Table 1 are used to construct selected binary plots. This method of presenting the data eliminates, to a large degree, the scatter that occurs when individual points from different localities are used. The compatible nature of Ir is demonstrated by the positive correlation between Ir and the fractionation indices, Ni and Mg#. Ir and Ru display systematic covariation throughout the entire range of rock types. Palladium, the most incompatible of the precious metals, displays a moderate negative correlation with Mg# and a moderate positive correlation with Au and Cu. The relatively large amount of scatter associated with the plots involving Pd, Au and Cu may reflect both the restricted range in concentration of these elements and their local redistribution during subsolidus alteration. The latter viewpoint is particularly valid for Cu, which locally occurs as secondary chrysocolla and native copper in altered cumulates and dykes, and is present as hydrothermal chalcocopyrite in many of the basalt samples.

In addition to the general trends described above, several additional features are evident from the study of covariance. In samples of dunite, Os, Ir, Ru and

Pd exhibit a weak to moderate positive correlation with loss-on-ignition (Table 3). This may reflect the higher degree of serpentinization in the most primitive rocks, and is supported by a moderate positive correlation between Ni and loss-on-ignition. This argument can be applied to the *IPGE*, which are enriched in the more primitive rocks, but not to Pd, which behaves incompatibly. It is possible, therefore, that some redistribution of Pd occurred during serpentinization. There is a weak negative correlation between loss-on-ignition and Pt and Pd abundances for the volcanic rocks (Table 4), which may also reflect redistribution of these elements during low-temperature alteration. In general, the lack of any strong correlation between loss-on-ignition and *PGE* abundances indicates that the precious metals were relatively inert during low-temperature alteration.

The spatial distribution of precious metals in the complex is reflected in the weighted mean abundances for the major sequences of cumulates (Table 2). These data relate to the overall degree of evolution of the sequences, defined by the relative abundances of the rock types. For example, the primitive 19 Mile Creek sequence is enriched in *IPGE*

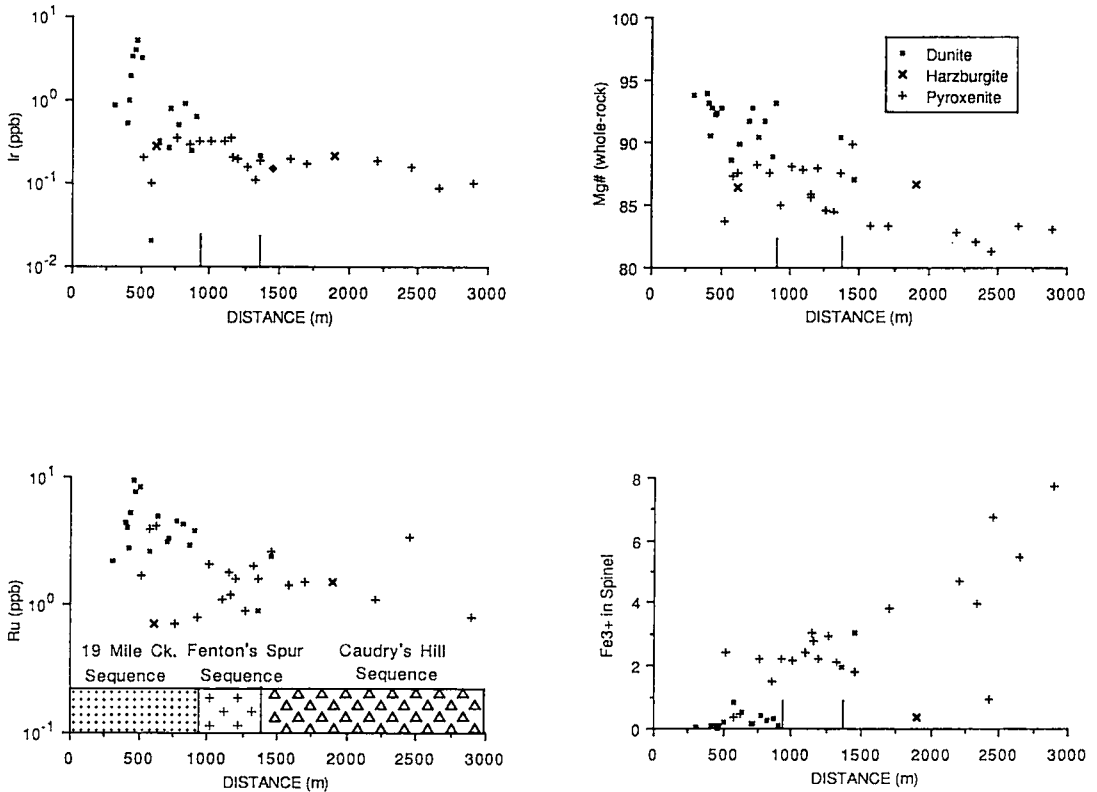


FIG. 8. Variations in whole-rock concentrations of Ir, Ru and Mg# and atomic proportions of Fe^{3+} in spinel (based on 24 cations and 32 oxygen atoms) along traverse A-A' (Fig. 2). The data are given in Appendix 2.

because of the high relative abundance of dunite. Similarly, the more evolved Purcell's Plain lherzolite sequence is relatively enriched in Pd, Au, Cu and S owing to a greater abundance of plagioclase-bearing rocks and higher porosities of the cumulates. One spatial anomaly for the PGE in the HRC involves the relatively high Pt abundances in the Fenton's Spur sequence (Table 2). Platinum concentrations in the vicinity of Fenton's Spur (Fig. 2) are commonly in excess of 30 ppb and are not restricted to a single rock type (Peck & Keays, unpublished data). This feature is illustrated by the high average Pt concentrations of several rock types from the Fenton's Spur dunite and pyroxenite sequences (Appendix 1), although these data also incorporate samples collected to the south of Fenton's Spur.

Several features distinguish the Fenton's Spur area from other parts of the complex. These include: (1) the presence of wehrlite in the Fenton's Spur pyroxenite sequence, (2) a relatively high modal abundance of chromite in the rocks (commonly 5–10%), (3) the presence of several magnetite-rich cumulate layers, locally containing 25% secondary magnetite, (4) the presence of talc-rich, deeply weathered cumulate

layers, and (5) a shallow dip of the igneous layering (commonly $<30^\circ$). Exploration of the area by Metals Exploration Ltd. has delineated several Pt-anomalies that warrant further investigation. The nature and origin of the high Pt abundances in the rocks remain unclear.

Detailed stratigraphic relationships within the cumulate sequences have proven difficult to establish owing to lack of outcrop in critical areas and the complexly faulted nature of the HRC. Samples collected along traverses normal to layering have provided some assistance in this regard. Compositional variations in spinel have allowed the recognition of at least one stratigraphic sequence. Traverse line A-A' (Fig. 2), which intersects the 19 Mile Creek dunite sequence, the Fenton's Spur sequence, the Caudry's Hill sequence and the Gabbro Hill sequence, appears to represent a continuous stratigraphic succession that is east-facing and incorporates the first three of the above-mentioned cumulate sequences. Data on the precious metals, selected trace elements and Cr-spinel composition for samples from traverse A-A' are given in Appendix 2.

Variations in whole-rock Mg# and Fe^{3+} content

of spinel along the traverse demonstrate an iron-enrichment trend (Fig. 8). Similar trends are defined by variations in silicate minerals along the traverse (Peck & Keays, unpublished data). Superimposed on the general trend toward more evolved geochemical compositions with increasing stratigraphic elevation are abrupt compositional reversals (Fig. 8). The latter are interpreted to reflect periods of magma replenishment. Although the relative abundance of orthopyroxenite increases up-sequence, the Fe-enrichment trend is clearly not related to rock-type variations alone. Ulmer (1969) demonstrated that the Fe^{3+} content of spinel is proportional to $f(\text{O}_2)$ in magmas. Therefore, the trend from extremely low Fe^{3+} in the 19 Mile Creek dunite sequence to extremely high Fe^{3+} in the upper part of the Caudry's Hill sequence (Fig. 8) is indicative of a progressive buildup in magmatic $f(\text{O}_2)$.

On the basis of layering styles and variations in whole-rock and mineral compositions (Peck & Keays, unpublished data), the western HRC has been interpreted to represent the cumulate products of two major magmatic cycles. The larger cycle gave rise to the 19 Mile Creek dunite sequence, the Fenton's Spur peridotite sequence and the Caudry's Hill pyroxenite sequence, and the smaller cycle produced the Gabbro Hill plagioclase pyroxenite sequence. Petrological and geochemical variations also suggest that the western HRC crystallized from a compositionally zoned magma chamber in which new injections of dense, primitive liquid remained at the floor of the intrusion and more evolved resident melt was displaced upward.

The *IPGE* are strongly enriched in the dunite-rich base of traverse A-A'. Plots of Ir and Ru abundances versus stratigraphic position (Fig. 8) show that a rapid buildup in *IPGE* concentrations occurs between 420 and 500 m and that Ir and, to a lesser extent, Ru concentrations experience an extreme and rapid decline immediately above 500 m. Osmium displays the same trend over this interval (Appendix 2). The rapid decline in *IPGE* abundances is followed by a return to higher values and a gradual, albeit somewhat erratic trend to lower concentrations at higher stratigraphic levels. Platinum, Pd and Au show no systematic variation with stratigraphic position (Appendix 2).

The variations in concentration of the precious metals along traverse A-A' are consistent with the *IPGE:PPGE* fractionation trends described previously. The limited and unsystematic behavior of Pt, Pd and Au reflects the incompatible behavior of these elements and the consistently low porosity (<10%) in the cumulate samples from the traverse. In contrast, the *IPGE* abundances are indicative of the compatible behavior of these elements, and can be generally linked to the increasingly evolved nature of the cumulates up-sequence. The sharp increase in

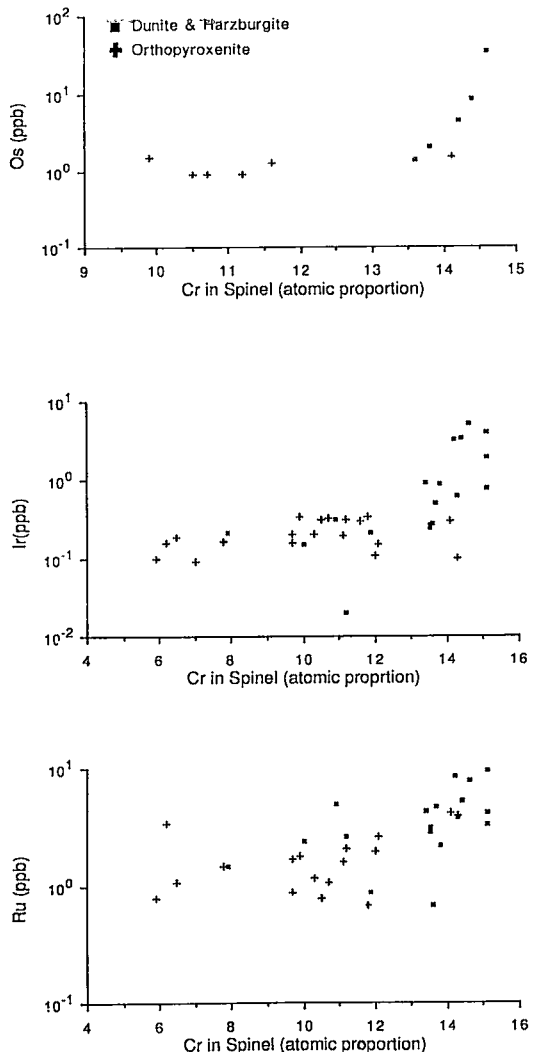


FIG. 9. Osmium, Ir and Ru concentrations versus atomic proportions of Cr in spinel (based on 24 cations and 32 oxygen atoms) for samples from traverse A-A'. The data are given in Appendix 2.

IPGE tenor in the basal dunite-rich sequence is interpreted to represent a major addition of primitive magma to the chamber. However, the good positive correlation between Os, Ir and Ru concentrations and Cr-content of spinel at high Cr abundances (Fig. 9) indicates that the *IPGE* were strongly partitioned into the most primitive dunite cumulates. It is interesting to note that several workings of alluvial "osmiridium" are spatially associated with these primitive dunites, and that the position of the hard-rock "osmiridium" workings on the west side of

Caudry's Hill (Fig. 2) corresponds to the peak in *IPGE* concentrations on traverse A-A'. These observations will be considered in more detail below.

DISCUSSION

Implications for the geochemistry of precious metals in primitive, S-undersaturated magmas

The observed fractionation of Os, Ir and Ru from Pt, Pd and Au during the crystallization of the Heazlewood River complex is a well-documented feature of ultramafic magmas (e.g., Agiorgitis *et al.* 1977, Barnes *et al.* 1985). A number of studies indicate that chromite is a major concentrator of *IPGE* (e.g., Gijbels *et al.* 1974, Stockman & Hlava 1984). A recent study of the *PGE* geochemistry of chromitites from the HRC (Peck & Keays 1990) has shown that they are enriched in *PGE*, particularly in Pt, Ru and Rh, relative to all other rock types. However, in the context of the present study, these chromitite-*PGM* occurrences can be considered as isolated and unusual phenomena that had little influence on the overall distribution of *PGE* in the HRC.

Chromite mineral separates, prepared from cumulates containing <1–2% disseminated spinel, are enriched in *PGE* relative to the silicate fraction of the host rock (Peck & Keays 1990). The chromite contributes 3–71% of the total Ir in the bulk samples. This corresponds to an enrichment factor of 4–180 for the chromite fraction relative to the silicate minerals. Similar enrichment trends are observed for Pt and Ru. These results indicate that chromite was locally an important concentrator of the *PGE*. The wide scatter in the *PGE* data from the chromite separates (Peck & Keays 1990) suggests that the disseminated chromite contains discrete inclusions of *PGM*. The latter may represent high-temperature *PGM* that were trapped by chromite during crystallization (e.g., Augé 1988) or, alternatively, the exsolution of *PGE* that were originally held in solid solution in the spinel structure (e.g., Gijbels *et al.* 1974, Naldrett & Cabri 1976).

Mineral separates of cumulus olivine obtained from komatiites that occur in the Kambalda area of Western Australia contain high abundances of Ir and account for the majority of the Ir in the rocks (Ross & Keays 1979, Keays 1982). This observation suggests that olivine may also play an important role in concentrating the *IPGE*. A number of other investigations have demonstrated that olivine mineral separates have a very low tenor of the *IPGE* (e.g., Gijbels *et al.* 1976, Mitchell & Keays 1981), but many of these studies deal with sulfide-bearing rocks, in which the *PGE* are preferentially partitioned into sulfide minerals. It therefore seems likely that both olivine and chromite can be effective concentrators of the *PGE* in S-undersaturated magmas.

The parental liquids for the HRC remained S-undersaturated during the formation of the layered sequences, dykes, and volcanic suites, as demonstrated above. We have shown that in these primitive liquids, the order of compatibility with early-formed cumulates increases in the order Pd < Au < Pt < Ru < Ir < Os, suggesting a strong thermodynamic control (i.e., melting point of the metal) on the solubility of the *PGE*. In the absence of cumulus sulfides, the more siderophile *PGE* are clearly capable of nucleating as discrete grains of *PGM*, as has been demonstrated experimentally (Amosse *et al.* 1987). These grains may be physically trapped by other cumulus phases, as indicated by the presence of *IPGE* minerals in spinel grains from primitive olivine-chromite cumulates in a number of ultramafic complexes (e.g., Stockman & Hlava 1984, Prichard *et al.* 1986, Augé 1988, Peck & Keays 1990).

The good positive correlation between chromite composition and whole-rock Os, Ir and Ru abundance (Fig. 9) clearly demonstrates that the *IPGE* are partitioned into the most primitive cumulates. This implies that *IPGE*-bearing minerals may have been concentrated during periods of magma replenishment. The fact that *IPGE*-enrichment is only observed in the most primitive sequence of cumulates (19 Mile Creek dunites) is evidence for a fractional crystallization - temperature control on the nucleation of *IPGE*-bearing minerals. A similar conclusion was reached by Tredoux *et al.* (1986) from their study of the *PGE* geochemistry of mafic and ultramafic rocks from the Kaapvaal Craton, South Africa.

Chromitites from the 19 Mile Creek dunite sequence are depleted in Ir (0.04 – 3.47 ppb; geometric mean 0.096 ppb; $n = 5$) and contain low Ru abundances (1.9 – 8.8 ppb; geometric mean 4.12 ppb; $n = 5$; Peck & Keays 1990) relative to dunite containing only disseminated spinel (Appendix 1). The chromitites contain much lower abundances of both Ir and Ru than would be expected given the significantly higher Ir and Ru values of chromite mineral separates from this sequence (3.5 – 26 ppb Ir; 24 – 69 ppb Ru; Peck & Keays, unpublished data). These features can be explained if chromitite formation postdated the extraction of the *IPGE* from the melt. The chromitites are interpreted to represent physical concentrations of chromite that may define replenishment events involving a chromite-saturated magma. The most primitive liquids in the HRC may have contained cumulus Os-Ir alloys that were concentrated along the floor of the chamber upon emplacement of the magma. Cumulates crystallizing from such a melt following Os-Ir alloy separation would have been depleted in these elements. The rapid rise and fall in *IPGE* abundances adjacent to the reported position of a hard-rock "osmiridium" lode (Twelvetrees 1914) along traverse A-A' (Fig.

8, Appendix 2) may reflect such an early separation of Os-Ir alloys.

Some indirect lines of evidence support this scenario. Amossé *et al.* (1987) demonstrated that Ir solubility decreases with increasing $f(O_2)$, and suggested that Ir-bearing minerals may nucleate prior to chromite. However, in the HRC the highest Os and Ir abundances occur in samples containing chromite with extremely low Fe^{3+} abundances, suggesting low $f(O_2)$. This apparent anomaly can be explained if the boninitic parental liquids were volatile-rich at their source (at which stage the Os-Ir alloys were formed), but upon ascent and emplacement, experienced a separation of the volatiles and a reduction in $f(O_2)$ (at which stage chromite crystallization occurred).

The high melting points of Os and Ir (3045 and 2410°C, respectively) are consistent with a high nucleation temperature for Os-Ir alloys. Ford (1981) found that primitive olivine, orthopyroxene and non-stoichiometric, Al-rich calcic pyroxene inclusions are present in Os-Ir-Ru alloys from alluvial deposits in Tasmania. The primitive compositions of the silicates led Ford to conclude that the alloys formed at extremely high temperatures (*i.e.*, in excess of 1300°C). The high Al content of many of the pyroxene inclusions indicates higher ambient pressures than those prevailing during the crystallization of the cumulate sequences, because the latter contain only low-Al pyroxenes (Brown 1986, Peck & Keays, unpublished data).

Recent exploration of the 19 Mile Creek dunite sequence for primary occurrences of Os-Ir alloys by Metals Exploration Ltd. failed to identify a bedrock source for the spatially associated alluvial "osmiridium" occurrences. Results from this study suggest that further detailed lithochemical investigation, such as that carried out along traverse A-A' (Fig. 2), must be undertaken in other parts of the sequence in order to delineate specific exploration targets. Variations in Cr-spinel compositions are probably the most important exploration tool because chromite is an excellent monitor of changes in magmatic $f(O_2)$, temperature and bulk composition. The results also suggest that chromitites are not necessarily important in concentrating the IPGE and that in boninitic magmas the crystallization and deposition of IPGE minerals may predate the formation of chromite-rich layers.

The negative Ir anomaly seen on the mantle-normalized plots (Fig. 4) cannot be explained by fractional crystallization of Os-Ir alloys, given that the majority of Tasmanian alloys are Os-rich (Ford 1981; R.J. Ford, pers. comm. 1987). The anomaly may reflect a pattern inherited from the source, early separation of an Ir-rich phase prior to emplacement of the primary liquids, or the selective removal of Os and Ru from the parental liquids. It is unclear

which mechanisms would allow preferential retention of Ir during partial melting. In addition, both Os and Ru can nucleate as disulfides (erlichmanite and laurite), whereas Ir crystallizes as Ir_2S_3 . Stockman & Hlava (1984) suggested that laurite containing 20 mole % OsS_2 will nucleate at a $f(S_2)$ below the Ir- Ir_2S_3 buffer. Therefore, nucleation of early IPGE-bearing sulfide would tend to remove Ru and Os and lead to a relative enrichment in Ir in residual liquids. The absence of Ir enrichment in the dykes and volcanic rocks argues against this process, given the assumption that some or all of these rocks are cogenetic with the cumulates, which indicates that an alternative process is required to account for the Ir anomaly.

The distributions of Pt, Pd and Au in the HRC are more easily understood. The incompatible behavior of these elements during the evolution of the HRC is attested to by their increasing abundances in more evolved rocks (Figs. 4, 6, 7, Table 1). An exception to this general trend involves the Pt enrichment, described above, for peridotites from the Fenton's Spur area. The factors responsible for the

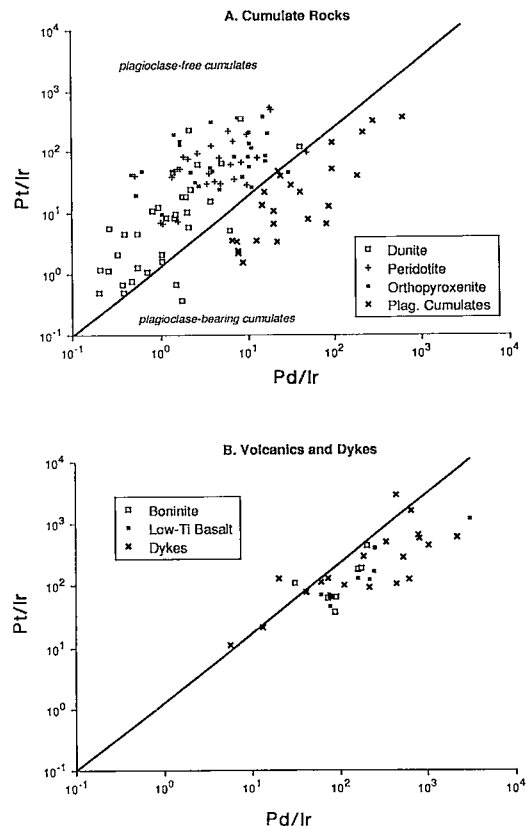


FIG. 10. Pt/Ir versus Pd/Ir plots for the Heazlewood River complex. Based on unpublished data (Peck & Keays).

anomalously high Pt abundances at this locality are poorly understood, but the area is clearly atypical of the cumulate portions of the complex. Figure 10 illustrates the incompatible nature of Pt and Pd in the HRC magmas. Both Pt/Ir and Pd/Ir increase from the most primitive cumulates (dunite) to more evolved rocks. However, the separation of the predominantly adcumulate plagioclase-free ultramafic rocks from the more porous plagioclase-bearing cumulates (Fig. 10A) is testimony to the much higher degree of incompatibility of Pd relative to Pt. The diagram may provide a useful means of discriminating between adcumulates and mesocumulates in highly altered terranes.

The noncumulate rocks have higher Pd/Ir and Pt/Ir values (Fig. 10B) and generally occur within the field of plagioclase-bearing cumulates defined in Figure 10A. Surprisingly, the boninites and many of the dykes plot together with the more evolved low-Ti tholeiitic basalts, indicating that the diagram is not a good discriminant for noncumulate rocks. This feature may reflect a gradual change in the behavior of Ir, from compatible in primitive magmas, to incompatible in more evolved liquids. This suggestion is supported by the U-shaped pattern on the plot of Ir versus Mg# for the major rock types in the complex (Fig. 7), which highlights an increase in Ir abun-

dance in the dykes and volcanic rocks below a Mg# of 75 (Fig. 4, Table 1).

The strongly incompatible behavior of Pd and Au in the parental magmas for the HRC explains the negative Pd and Au anomalies in the cumulate rocks (Fig. 4). Given the S-undersaturated nature of boninites and low-Ti lavas (Hamlyn *et al.* 1985, this study), the most chalcophile precious metals (Pt, Pd and Au) should experience a steady increase during fractional crystallization. Therefore, evolved boninitic liquids represent an extremely fertile magma for the formation of *PPGE*-Au mineralization. In the case of the HRC, these fertile magmas did not reach S-saturation, either through contamination, magma mixing or fractional crystallization, and hence their great potential for generating *PPGE* deposits remained untapped. This result supports the suggestion of Sun (1990) that although both low-Ti lavas and komatiitic lavas are similarly fertile with respect to the *PGE*, the stable cratonic environment into which komatiitic melts were emplaced is more favorable for generating the conditions necessary for the formation of *PGE* deposits.

Comparison with other mafic-ultramafic complexes

Brown *et al.* (1988) determined *PGE* abundances

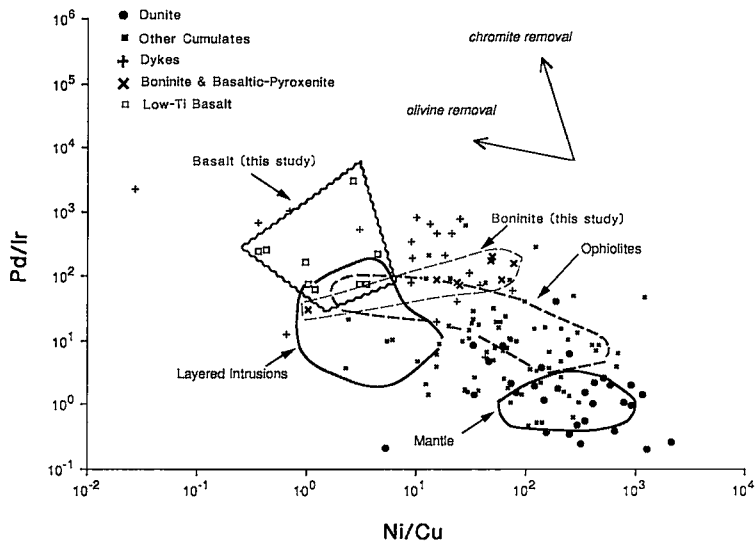


FIG. 11. Pd/Ir versus Ni/Cu metal ratio diagram (after Barnes *et al.* 1988) for the Heazlewood River complex. The data points are derived from unpublished analyses (Peck & Keays). Field boundaries for mantle, layered intrusions and ophiolites, and mineral-control vectors, are taken from Barnes *et al.* (1988, Fig. 3). Field boundaries for boninite and low-Ti tholeiitic basalt are based on the displayed data from this study. Symbols: circles: dunite, closed squares: all other cumulates, crossed diagonals: boninite and basaltic pyroxenite dykes, large open squares: low-Ti tholeiitic basalt, horizontal crosses: gabbro and anorthosite dykes.

in 10 samples of ultramafic cumulates from the LDH sequence of the HRC, and reported Pt values between 11 and 21 ppb. All other PGE were below the detection limits for the fire-assay - atomic absorption method that they employed. These Pt abundances are higher than those given in Table 2 for the 19 Mile Creek dunite sequence (LDH correlate). Brown *et al.* (1988) reported Pt abundances for cumulate rocks from the Serpentine Hill complex (Fig. 2) that are higher than the majority of samples from other mafic-ultramafic complexes in Tasmania, including data from the present study. This result may reflect the more evolved nature of the Serpentine Hill complex, which contains a much higher proportion of cumulate gabbro than the HRC, and is consistent with the predicted incompatible behavior of Pt during the formation of these complexes.

The PGE abundances of the major rock types from the HRC were compared to those in a number of other mafic-ultramafic complexes, including ophiolites and alpine-type peridotites, large stratiform intrusions and Alaskan-type complexes. The strong influence of the degree of partial melting and fractional crystallization on the absolute abundances of precious metals in ultramafic rocks (*e.g.*, Hamlyn & Keays 1986, Barnes *et al.* 1985) makes the use of elemental ratios imperative. One such ratio, Pt/(Pt + Pd), has been successfully used to discriminate among ultramafic rocks from different tec-

tonic settings. Naldrett & Cabri (1976) gave average Pt/(Pt + Pd) values of 0.87 for alpine peridotites (Urals), which is similar to average values for dunite, harzburgite and orthopyroxenite from the present study (0.82, 0.91 and 0.91, respectively, derived from Table 1). However, the much lower values for more evolved rock-types from the HRC, including troctolite (0.73), plagioclase pyroxenite (0.67) and plagioclase peridotite (0.54), indicate that this ratio is very sensitive to porosity of the cumulates and decreases during fractional crystallization.

The diagram showing Pd/Ir versus Ni/Cu ratio, first proposed by Barnes *et al.* (1985), provides another discriminant of the tectonic association of ultramafic rocks; as well, it allows recognition of evolutionary trends for cogenetic igneous suites. The metal ratio diagram for the HRC (Fig. 11) highlights the extremely primitive nature of the complex. Dunite samples plot within the mantle field; the majority of the remaining samples fall in or adjacent to the ophiolite field. The diagram also illustrates that the boninites are much more primitive than the basalts. The metal ratios indicate that the latter can only be related to the cumulates through extensive fractional crystallization of olivine. In contrast, the boninites have metal ratios similar to many of the more evolved cumulates, and require only limited fractional crystallization, principally involving chromite removal, in order to be linked to the

TABLE 5. COMPARISON OF AVERAGE PRECIOUS METAL ABUNDANCES OF THE HEAZLEWOOD RIVER COMPLEX AND SELECTED ULTRAMAFIC COMPLEXES

| HEAZLEWOOD RIVER COMPLEX-CUMULATES | | | | | | | | | |
|-------------------------------------|-----|-------|-----|-----|-----|-----|------|-------|-------|
| | Os | Ir | Ru | Rh | Pt | Pd | Au | Pd/Ir | Pt/Ir |
| Dunite | 7.9 | 0.62 | 3.2 | - | 2.9 | 0.6 | 0.13 | 1.0 | 4.68 |
| Orthopyroxenite | 0.7 | 0.15 | 1.4 | - | 6.2 | 0.6 | 0.08 | 4.0 | 41.3 |
| Plag. Peridotite | - | 0.17 | 1.1 | - | 6.0 | 5.1 | 0.31 | 30.0 | 35.3 |
| Weighted Mean | 3.2 | 0.32 | 2.1 | - | 6.1 | 1.0 | 0.12 | 3.1 | 19.1 |
| TULAMEEN COMPLEX (ALASKAN) | | | | | | | | | |
| Dunite and Peridotite | - | 0.5 | - | 1.2 | 48 | - | 0.29 | - | 96.0 |
| (Olivine) Clinopyroxenite | - | 2.7 | - | 0.8 | 30 | - | 0.4 | - | 11.1 |
| Weighted Mean | 0.5 | 0.4 | - | 0.4 | 120 | 30 | 1.5 | 75.0 | 300 |
| THETFORD MINES OPHIOLITES-CUMULATES | | | | | | | | | |
| Dunite | - | 2.4 | - | - | 28 | 21 | 1.3 | 8.75 | 11.7 |
| Pyroxenite | - | 0.24 | - | - | 17 | 29 | 1.4 | 121 | 70.8 |
| Gabbro | - | 0.017 | - | - | 4.5 | 3.0 | 1.7 | 176 | 265 |
| STILLWATER COMPLEX-BELOW J-M REEF | | | | | | | | | |
| Average Mafic Cumulate | - | 0.17 | - | - | 13 | 7 | 0.4 | 41.2 | 76.5 |

Notes: All data represent mean whole-rock abundances in ppb. Ratios are derived from the data in the table. Weighted mean abundances are based on the estimated volume % of all rock types. Weightings for the HRC are: Dunite 30%; Harzburgite 25%; Orthopyroxenite 30%; Wehrlite 2%; Troctolite 3%; Plagioclase Peridotite 5%; Plagioclase Pyroxenite 5%. Data Sources: HRC: Table 1, this study; Tulameen Complex: St. Louis *et al.* (1986); Thetford Mines Ophiolites: Oshin & Crockett (1982); Stillwater Complex: P.R. Hamlyn, personal communication 1989.

most primitive cumulates in the HRC (Fig. 11).

PGE data for type examples for ultramafic intrusions from different tectonic settings are given in Table 5. These examples were selected because they provide detailed *PGE* data on rocks that do not contain *PGE*-chromitite or *PGE*-sulfide mineralization. The comparison highlights the extremely low Pd abundances and high relative tenor of *IPGE* in the HRC cumulates. The weighted mean Pd/Ir and Pt/Ir values for the HRC are much lower than those for the Tulameen Complex and the lower parts of the Stillwater Complex, but similar to cumulate dunite and peridotite from the Thetford Mines ophiolite. The results of these comparisons provide a general indication that the HRC has similarities to ophiolites in terms of distribution of the precious metals.

The parental liquids for the cumulate sequences are considered to have been cogenetic with the boninite and low-Ti tholeiite lavas that flank the ultramafic portion of the HRC. Brown (1986) established geochemical links between these two volcanic suites and the cumulate sequences from several of the Tasmanian mafic-ultramafic complexes. The boninite and low-Ti tholeiitic lavas from the present study display similar relative and absolute abundances of the precious metals. This result is consistent with the suggestion of Brown & Jenner (1989) that the two suites represent partial melts derived from a broadly similar mantle source. However, some important geochemical differences between the low-Ti basalt and boninite lavas have been documented in the present study. Foremost of these are the lower absolute Pd and TiO₂ abundances and higher Ni/Cu ratios and Mg# of the boninite samples. These results indicate that the boninite lavas are far more primitive than the basaltic rocks and are more likely to represent a parental magma for the cumulates.

The volcanic rocks of the HRC are chemically and petrologically analogous to Mg-rich lavas in several ophiolite complexes (*e.g.*, Troodos, Betts Cove; Crawford *et al.* 1989) and have precious metal concentrations that are strikingly similar to low-Ti lavas derived from partial melting of refractory, lithospheric mantle (Hamlyn *et al.* 1985). The latter observation represents new evidence in support of the proposed association between the Tasmanian mafic-ultramafic complexes and arc-related magmatism involving second-stage melts (Berry & Crawford 1988, Brown & Jenner 1989). The trends in the distribution of the precious metals described here should be applicable to primitive, S-undersaturated magmas in general.

CONCLUSIONS

The results of this investigation indicate that Os, Ir and Ru were partitioned into early-formed cumu-

lates, and Pt, Pd and Au remained in residual liquids during the crystallization of the HRC. The precious metals display the following affinity for primitive cumulates, in order of increasing compatibility: Pd < Au < Pt < Ru < Ir < Os. This sequence illustrates the influence of melting point on the solubility of the *PGE* and Au in primitive magmas (Tredoux *et al.* 1986).

The observed enrichment in *IPGE* in the 19 Mile Creek dunite sequence may be related to the precipitation of Os-Ir (\pm Ru) alloys, which would account for the presence of spatially associated alluvial "osmiridium" deposits. The positively sloping mantle-normalized precious metal patterns of boninite and low-Ti tholeiitic basalt samples from the HRC are a consequence of the range of compatibility displayed by the *PGE* and Au during fractional crystallization. Negative Ir anomalies appear to reflect the decoupling of Ir from Os and Ru during partial melting or fractional crystallization. Negative Pd and Au anomalies in the cumulate rocks are a consequence of the extremely incompatible behavior of these elements in S-poor magmas. The strong Pt-enrichment in peridotite samples from the HRC is indicative of high Pt abundances in cumulates from a single locality (Fenton's Spur).

Despite being derived from S-impoverished, *PGE*-enriched second-stage melts, the HRC is not a likely prospect for stratiform *PGE*-sulfide mineralization owing to the failure of these liquids to reach S-saturation. The distribution of precious metals in the HRC compares most favorably with that in ophiolites. The results of this study should be applicable to ophiolites having boninitic affinities and to S-undersaturated ultramafic magmas in general.

ACKNOWLEDGEMENTS

The authors express their appreciation to Metals Exploration Ltd. and, in particular, to Messrs. S. Carthew and T. Summons, for logistical and technical support and for permission to publish this material. We acknowledge the technical assistance provided by S. J. Reeves, C. A. Peck, M. T. Haukka, D. K. B. Sewell, and P. Kelly. The project was supported by a Melbourne University Postgraduate Scholarship awarded to D.C.P., and by grants received from the ARGs, AINSE and AMIRA. The manuscript was improved by criticisms made by Drs. A. V. Brown and Sarah-Jane Barnes.

REFERENCES

- AGIORGITIS, G., BECKER, R. & WOLF, R. (1977): Aspects of platinum elements distribution in some ultramafic and related rocks. *In* Origin and Distribution of the Elements (L.H. Ahrens, ed.). Pergamon Press, Oxford, United Kingdom (233-238).

- AMOSSÉ, J., ALLIBERT, M., FISCHER, W. & PIBOULE, M. (1987): Étude de l'influence des fugacités d'oxygène et de soufre sur la différenciation des platinoïdes dans les magmas ultramafiques: résultats préliminaires. *C. R. Acad. Sci. Paris* **304**, Sér. II, 1183-1185.
- AUGÉ, T. (1988): Platinum-group minerals in the Tiébaghi and Vourinos ophiolitic complexes: genetic implications. *Can. Mineral.* **26**, 177-192.
- BARNES, S.-J., BOYD, R., KORNELIUSSEN, A., NILSSON, L.-P., OFTEN, M., PEDERSEN, R.B. & ROBINS, B. (1988): The use of mantle normalization and metal ratios in discriminating between the effects of partial melting, crystal fractionation and sulfide segregation on platinum-group elements, gold, nickel and copper: examples from Norway. *In Geo-Platinum '87 Symp. Vol.* (H.M. Prichard, P.J. Potts, J.F.W. Bowles & S.J. Cribb, eds.). Elsevier, London (113-143).
- , NALDRETT, A.J. & GORTON, M.P. (1985): The origin of the fractionation of platinum-group elements in terrestrial magmas. *Chem. Geol.* **53**, 303-323.
- BERRY, R.F. & CRAWFORD, A.J. (1988): The tectonic significance of Cambrian allochthonous mafic-ultramafic complexes in Tasmania. *Aust. J. Earth Sci.* **35**, 523-533.
- BROWN, A.V. (1986): Geology of the Dundas - Mt. Lindsay - Mt. Youngbuck region. *Geol. Surv. Tasmania Bull.* **62**.
- & JENNER, G.A. (1989): Geological setting, petrology and chemistry of Cambrian boninite and low-Ti tholeiite lavas in western Tasmania. *In Boninites and Related Rocks* (A.J. Crawford, ed.). Unwin Hyman, London (236-263).
- , PAGE, N.J. & LOVE, A.H. (1988): Geology and platinum-group element geochemistry of the Serpentine Hill Complex, Dundas Trough, western Tasmania. *Can. Mineral.* **26**, 161-175.
- CORBETT, K.D. & LEES, T.C. (1987): Stratigraphic and structural relationships and evidence for Cambrian deformation at the western margin of the Mount Read volcanics, Tasmania. *Aust. J. Earth Sci.* **34**, 45-67.
- CRAWFORD, A.J., FALLOON, T.J. & GREEN, D.H. (1989): Classification, petrogenesis and tectonic setting of boninites. *In Boninites and Related Rocks* (A. J. Crawford, ed.). Unwin Hyman, London (1-49).
- CREENAUNE, P. (1980): *The Volcanics of the Heazlewood River Complex*. B.Sc. thesis, Univ. Tasmania, Hobart, Tasmania.
- ECKSTRAND, O.R. (1975): The Dumont serpentinite: a model for control of nickeliferous opaque assemblages by alteration reactions in ultramafic rocks. *Econ. Geol.* **70**, 183-201.
- FORD, R.J. (1981): Platinum-group minerals in Tasmania. *Econ. Geol.* **76**, 498-504.
- GIJBELS, R., HENDERSON, P. & ZELS, J. (1976): Geochemistry of some trace elements in mineral separates from Rhum, Inner Hebrides, with special emphasis on iridium. *Econ. Geol.* **71**, 1364-1370.
- , MILLARD, H.T., DESBOROUGH, G.A. & BARTEL, A.J. (1974): Osmium, ruthenium, iridium and uranium in silicates and chromite from the eastern Bushveld Complex, South Africa. *Geochim. Cosmochim. Acta* **38**, 319-337.
- HAMLIN, P.R. & KEAYS, R.R. (1986): Sulfur-saturation and second-stage melts: application to the Bushveld platinum metal deposits. *Econ. Geol.* **81**, 1431-1445.
- , ———, CAMERON, W.E., CRAWFORD, A.J. & WALDRON, H.M. (1985): Precious metals in magnesian low-Ti lavas: implications for metallogenesis and sulfur-saturation in primary magmas. *Geochim. Cosmochim. Acta* **49**, 1797-1811.
- HAUGHTON, D.R., ROEDER, P.L. & SKINNER, B.J. (1974): Solubility of sulfur in magmas. *Econ. Geol.* **69**, 451-467.
- HAUKKA, M.T. & THOMAS, I.L. (1977): Total X-ray fluorescence analysis of geological samples using a low-dilution lithium metaborate fusion method. Matrix corrections for major elements. *X-ray Spectrometry* **6**, 204-211.
- HOATSON, D.M. & KEAYS, R.R. (1990): Formation of platiniferous sulfide horizons by crystal fractionation and magma mixing in the Munni Munni layered intrusion, West Pilbara Block, Western Australia. *Econ. Geol.* (in press).
- HOWARD, J.H., III (1977): Geochemistry of selenium: formation of ferroselite and selenium behavior in the vicinity of oxidizing sulfide and uranium deposits. *Geochim. Cosmochim. Acta* **41**, 1665-1678.
- JENNINGS, I.B., NOLDART, A.J. & WILLIAMS, E. (1967): Geology and mineral resources of Tasmania. *Geol. Surv. Tasmania Bull.* **50**.
- KEAYS, R.R. (1982): Palladium and iridium in komatiites and associated rocks: application to petrogenetic problems. *In Komatiites* (N.T. Arndt & E.G. Nisbet, eds.). George, Allen and Unwin, London (435-457).
- MANN, B. (1988): *The Geology of Brassey Hill. The Nature and Genesis of Nickel Mineralization at the Heazlewood River Complex, Tasmania*. B.Sc. thesis, Univ. Melbourne, Parkville, Victoria, Australia.

- MERTIE, J.B. (1969): Economic geology of the platinum-group metals. *U.S. Geol. Surv., Prof. Pap.* **630**.
- MITCHELL, R.H. & KEAYS, R.R. (1981): Abundance and distribution of gold, palladium and iridium in some spinel and garnet lherzolites: implications for the nature and origin of precious metal-rich intergranular components in the upper mantle. *Geochim. Cosmochim. Acta* **45**, 2425-2442.
- NALDRETT, A.J. & CABRI, L.J. (1976): Ultramafic and related rocks: their classification and genesis with special reference to their concentration of nickel sulfides and platinum-group elements. *Econ. Geol.* **71**, 1131-1158.
- NYE, P.B. (1929): The osmiridium deposits of the Adamsfield district. *Geol. Surv. Tasmania Bull.* **39**.
- OSHIN, I.O. & CROCKET, J.H. (1982): Noble metals in Thetford ophiolites, Quebec, Canada. 1. Distribution of gold, iridium, platinum and palladium in the ultramafic and gabbroic rocks. *Econ. Geol.* **77**, 1556-1570.
- PAGE, N.J. & TALKINGTON, R.W. (1984): Palladium, platinum, rhodium, ruthenium and iridium in peridotites and chromitites from ophiolite complexes in Newfoundland. *Can. Mineral.* **22**, 137-149.
- PECK, D.C. & KEAYS, R.R. (1990): Geology, geochemistry and origin of platinum-group element — chromitite occurrences in the Heazlewood River complex, Tasmania. *Econ. Geol.* (in press).
- PRICHARD, H.M., NEARY, C.R. & POTTS, P.J. (1986): Platinum-group minerals in the Shetland ophiolite. In *Metallogeny of Basic and Ultrabasic Rocks* (M.J. Gallagher, R.A. Ixer, C.R. Neary & H.M. Prichard, eds.). Inst. Mining Metall., London (395-414).
- REID, A.M. (1920): Osmiridium in Tasmania. *Geol. Surv. Tasmania Bull.* **32**.
- ROSS, J.R. & KEAYS, R.R. (1979): Precious metals in volcanic-type nickel sulfide deposits in Western Australia. 1. Relationship with the composition of the ores and their host rocks. *Can. Mineral.* **17**, 417-435.
- RUBENACH, M.J. (1973): *The Tasmanian Ultramafic Gabbro and Ophiolite Complexes*. Ph.D. thesis, Univ. Tasmania, Hobart, Tasmania.
- (1974): The origin and emplacement of the Serpentine Hill complex, western Tasmania. *J. Geol. Soc. Aust.* **21**, 91-106.
- SOLOMON, M. & GRIFFITHS, J.R. (1972): Tectonic evolution of the Tasman Orogenic Zone, eastern Australia. *Nature Phys. Sci.* **237**(70), 3-6.
- ST. LOUIS, R.M., NESBITT, B.E. & MORTON, R.D. (1986): Geochemistry of platinum-group elements in the Tulameen ultramafic complex, southern British Columbia. *Econ. Geol.* **81**, 961-973.
- STOCKMAN, H.W. & HLAVA, P.F. (1984): Platinum-group minerals in alpine chromitites from southwestern Oregon. *Econ. Geol.* **79**, 491-508.
- SUN, SHEN-SU (1990): Mantle plume and melting of refractory mantle: implications for PGE and Au mineralization. In *Tenth Australian Geological Convention, Abstracts Vol.*, Geol. Soc. Australia (130).
- TREDOUX, M., DAVIES, G., LINDSAY, N.M. & SELLSCHOP, J.P.F. (1986): The influence of temperature on the geochemistry of the platinum-group elements and gold. In *Geocongress 86*, Johannesburg, South Africa (625-628).
- TWELVETREES, W.H. (1914): The Bald Hill osmiridium field. *Geol. Surv. Tasmania Bull.* **17**.
- ULMER, G.C. (1969): Experimental investigations of chromite spinels. In *Magmatic Ore Deposits* (H.D.B. Wilson, ed.). *Econ. Geol., Monogr.* **4**, 114-131.
- VARNE, R. & BROWN, A.V. (1978): The geology and petrology of the Adamsfield ultramafic complex, Tasmania. *Contrib. Mineral. Petrol.* **67**, 195-207.
- & FODEN, J.D. (1987): Tectonic setting of Cambrian rifting, volcanism and ophiolite formation in western Tasmania. *Tectonophysics* **140**, 275-295.
- WILLIAMS, E. (1978): Tasman fold belt system in Tasmania. *Tectonophysics* **48**, 159-205.

Received February 20, 1990, revised manuscript accepted June 11, 1990.

APPENDIX 1. MEAN ABUNDANCES OF PRECIOUS METALS AND TRACE ELEMENTS FOR THE MAJOR CUMULATE SEQUENCES IN THE HEAZLEWOOD RIVER COMPLEX

| UNIT | TYPE | Weighting | Os | Ir | Ru | Pt | Rh | Au | Ni | Cu | S | Mg # | Pt/Ir | Pd/Pd |
|-----------------|-----------------|-----------|----------------|-------------------|-----------------|----------------|-----------------|-------------------|---------------|----------------|----------------|----------------|----------------|----------------|
| NM | DUN | 0.80 | 7.86±1.08 (7) | 0.803±1.39 (24) | 3.99±2.25 (24) | 1.29±3.41 (24) | 0.59±0.39 (18) | 0.109±0.071 (24) | 2430±281 (24) | 6.95±15.3(23) | 36.3±18.1 (11) | 92.1±1.42 (24) | 1.61±24.9 (24) | 2.20±2.71 (18) |
| | | range | 2.1-34.0 | 0.02-5.09 | 0.6-9.5 | 0.2-14.9 | 0.3-1.3 | 0.02-0.36 | 1890-2960 | <1-78 | <20-86 | <20-27 | 88.7-94.0 | 0.06-120 |
| HAR | HAR | 0.10 | 1.4 (1) | 0.28 (1) | 0.7 (1) | 4.8 (1) | - | 0.30 (1) | 1190 (1) | 4 (1) | 105 (1) | 86.4 (1) | 17.1 (1) | - |
| | | range | - | - | - | - | - | - | - | - | - | - | - | - |
| OPX | OPX | 0.10 | 0.25±0.779 (4) | 0.104±0.141 (7) | 1.65±1.56 (6) | 4.76±2.82 (7) | 0.21±2.283 (4) | 0.145±0.143 (7) | 757±188 (7) | 4.42±4.32 (6) | 26.0±1.00 (3) | <20-27 | 87.5±1.86 (7) | 45.7±133 (7) |
| | | range | <0.1-1.5 | 0.01-0.35 | <0.4-4.2 | 0.8-8.5 | 0.1-0.7 | 0.04-0.44 | 628-1160 | <1-13 | <20-27 | <20-27 | 83.7-89.4 | 10.3-385 |
| FS(dn) | DUN | 0.60 | - | 0.806 (2) | 2.02 (2) | 2.14 (2) | 0.572 (2) | 0.223 (2) | 1980±148 (3) | 31.3±227 (3) | 35.0 (2) | 87.9±0.71 (3) | 2.65 (2) | 4.09 (2) |
| | | range | - | 0.34-1.91 | 1.8-2.3 | 2.0-2.3 | 0.4-0.7 | 0.16-0.31 | 1820-2110 | 3-408 | <20-41 | <20-41 | 87.3-88.7 | 1.21-5.82 |
| HAR | HAR | 0.30 | - | 0.35 (1) | 1.1 (1) | 16.0 (1) | 0.5 (1) | 0.16 (1) | 1250 (1) | 98 (1) | 45 (1) | 87.5 (1) | 45.7 (1) | 32.0 (1) |
| | | range | - | - | - | - | - | - | - | - | - | - | - | - |
| OPX | OPX | 0.10 | 2.8 (1) | 0.22 (1) | 2.7 (1) | 78.9 (1) | 1.7 (1) | 0.10 (1) | 557 (1) | 9 (1) | - | 85.2 (1) | 359 (1) | 46.4 (1) |
| | | range | - | - | - | - | - | - | - | - | - | - | - | - |
| FS(upt) | DUN | 0.20 | - | 0.307±0.165 (4) | 2.62±1.41 (4) | 37.6±57.9 (4) | 1.05±0.892 (4) | 0.261±0.080 (4) | 1520±217 (4) | 33.3±11.6 (4) | 37.1 (2) | 84.5±1.17 (4) | 122±146 (4) | 36.3±40.2 (4) |
| | | range | - | 0.14-0.53 | 1.3-4.2 | 8.8-120 | 0.6-2.5 | 0.23-0.30 | 1240-1740 | 20-48 | <20-46 | 82.8-85.5 | 44.8-333 | 12.6-105 |
| HAR | HAR | 0.25 | - | 0.28±0.087 (3) | 1.28±0.745 (3) | 16.1±2.07 (3) | 0.50±0.0896 (3) | 0.21±0.0625 (3) | 1150±147 (3) | 48.5±5.5 (3) | 26-109 | 85.5±1.92 (3) | 57.5±12.8 (3) | 32.4±2.38 (3) |
| | | range | - | 0.19-0.35 | 0.6-2.0 | 13.9-17.9 | 0.4-0.6 | 0.15-0.27 | 989-1280 | 34-96 | 26-109 | 83.4-87.2 | 50.9-73.2 | 30.0-34.8 |
| WHEER + LHER | WHEER + LHER | 0.15 | - | 0.17±0.0900 (10) | 1.54±0.733 (10) | 31.3±12.6 (10) | 0.98±0.689 (8) | 0.193±0.147 (8) | 784±143 (11) | 26.2±37.8 (11) | 33.0±20.1 (5) | 85.7±2.09 (11) | 182±160 (10) | 29.6±8.47 (8) |
| | | range | - | 0.05-0.33 | 0.6-2.9 | 19.1-53.2 | 0.4-2.6 | 0.11-0.50 | 514-1030 | 13-144 | <20-70 | 81.7-88.5 | 83.0-537 | 19.2-45.5 |
| OPX + WEBB | OPX + WEBB | 0.40 | 1.18±0.537 (5) | 0.240±0.0894 (13) | 1.47±0.607 (13) | 7.66±24.6 (13) | 0.382±0.227 (6) | 0.118±0.165 (13) | 735±156 (13) | 71.3±79.8 (11) | 29.1±10.1 (8) | 85.8±1.50 (13) | 31.9±93.1 (13) | 61.5±40.5 (6) |
| | | range | 0.3-2.1 | 0.11-0.37 | 0.8-2.8 | 0.3-88.1 | <0.2-0.7 | 0.03-0.56 | 387-887 | <1-271 | <20-54 | 83.6-88.1 | 2.00-302 | 9.67-136 |
| CH(upt) | DUN | 0.10 | - | 0.182 (2) | 1.47 (2) | 4.70 (2) | 0.4 (1) | 0.0346 (2) | 1810 (2) | 2.83 (2) | 66.4 (2) | 88.8 (2) | 26.4 (2) | 23.0 (1) |
| | | range | - | 0.15-0.22 | 0.9-2.4 | 2.5-9.2 | - | 0.03-0.04 | 1560-2060 | 2-4 | 24-184 | 87.1-90.4 | 11.4-61.3 | - |
| HAR | HAR | 0.05 | - | 0.22 (1) | 1.5 (1) | 1.2 (1) | - | 0.04 (1) | 1790 (1) | 3 (1) | 45 (1) | 87.5 (1) | 5.45 (1) | - |
| | | range | - | - | - | - | - | - | - | - | - | - | - | - |
| OPX | OPX | 0.85 | 0.4 (1) | 0.179±0.0200 (5) | 1.57±0.368 (5) | 2.47±1.78 (5) | 0.433±0.367 (4) | 0.056±0.0319 (5) | 902±238 (5) | 4.50±12.5 (5) | 50.1±8.06 (5) | 85.4±3.18 (5) | 13.8±9.04 (5) | 7.82±15.5 (4) |
| | | range | - | 0.15-0.20 | 1.1-2.6 | 0.7-5.2 | <0.5-2.2 | 0.04-0.11 | 631-1200 | 1-31 | <20-58 | 82.8-89.9 | 4.67-26.0 | 2.36-36.0 |
| CH(ve) | OPX | 0.50 | - | 0.113±0.0380 (3) | 1.65 (2) | 4.49±0.361 (3) | 0.318±0.115 (3) | 0.0788±0.0173 (3) | 674±87.2 (6) | 8.00±9.04 (6) | 51.5±17.9 (3) | 83.0±1.31 (6) | 39.8±9.1 (3) | 14.1±5.06 (3) |
| | | range | - | 0.09-0.16 | <0.6-3.4 | 4.1-4.8 | 0.2-0.4 | 0.07-0.10 | 598-841 | 1-27 | <20-74 | 81.3-85.1 | 30.0-46.0 | 11.5-20.5 |
| PL WEBB | PL WEBB | 0.50 | - | 0.142±0.0252 (3) | 0.75±0.404 (3) | 5.70±3.20 (3) | 1.63±1.10 (3) | 0.387±0.390 (3) | 564±253 (6) | 13.2±8.68 (6) | 47.0±9.00 (4) | 79.9±1.86 (6) | 40.1±9.10 (3) | 3.50±5.92 (3) |
| | | range | - | 0.12-0.17 | 0.40-1.20 | 3.4-9.7 | 0.17-1.89 | 280-1040 | 6-36 | <20-56 | 77.1-82.8 | 20.0-80.8 | 1.87-12.1 | |

Notes: Average values represent geometric means for the PGE, Pt/Ir and Pd/Ru and arithmetic means for trace elements and Mg#. Mg# = 100Mg/(Mg+Fe²⁺) where total iron is reported as FeO. Platinum-group element data are in ppb. Nickel, Cu and S are in ppm. Standard deviation based on N-1 (t sign). Values in parentheses are the number of analyses above the detection limit, from which the mean and standard deviation were calculated. Weighting values are estimates of the relative proportions of the major rock types in the cumulate sequences. Abbreviations: LHER=liherzuite; WEBB=websterite; all other abbreviations as per Tables 1 and 2.

| UNIT | TYPE | Weighting | On | F | Ru | Ri | Rl | Ru | Ni | Cu | S | Mg # | Pt/F | Pt/Pd |
|----------|-------|-----------|------------------|-------------------|-----------------|----------------|--------------------|--------------------|---------------|----------------|----------------|----------------|-----------------|----------------|
| CH(6) | DUN | mean | - | 0.25840.104 (3) | 1.4084.551 (3) | 4.4341.07 (3) | - | 0.043144.00577 (3) | 1404.190 (3) | 3.7841.73 (3) | 59.425.8 (3) | 88.243.05 (3) | 17.245.3 (3) | - |
| | | range | - | 0.21-0.39 | 1.1-2.1 | 0.9-2.10 | - | 0.04-0.05 | 1210-1590 | 3-6 | 34-81 | 84.8-90.6 | 4.29-100 | - |
| HAR | mean | - | 0.13830.0300 (3) | 2.2640.987 (3) | 7.5824.64 (3) | 0.592 (2) | 0.063144.04946 (3) | 1188.208 (3) | 4.69 (2) | 40.643.1 (3) | 85.642.30 (3) | 54.341.0.3 (3) | 10.5 (2) | - |
| | | range | - | 0.11-0.17 | 1.7-3.5 | 6.0-10.8 | <0.3-0.7 | 0.04-0.12 | 967-1370 | <1-11 | 36-42 | 83.0-87.9 | 42.9-63.5 | 9.29-12.0 |
| OPX | mean | - | 0.183 (2) | 1.08 (2) | 4.21 (2) | 2.2 (1) | 0.0424 (2) | 5.51 (2) | 2 (1) | 34.5 (2) | 89.2 (2) | 2.9 (2) | 5.36 (1) | - |
| | | range | - | 0.16-0.21 | 0.9-1.3 | 1.5-11.8 | - | 0.03-0.06 | 484-617 | - | 34-35 | 85.3-93.1 | 9.38-56.2 | - |
| CH(6) | OPX | mean | - | 0.041240.0458 (3) | 0.86040.346 (3) | 4.9344.14 (3) | 1.32 (2) | 0.037840.0379 (3) | 441.244 (3) | 5.0646.25 (3) | 30.6410.6 (3) | 84.041.48 (3) | 120.582 (3) | 2.56 (2) |
| | | range | - | 0.01-0.10 | 0.7-1.3 | 2.6-10.5 | 0.6-2.9 | 0.02-0.09 | 421-468 | 1-1.3 | <20-39 | 82.3-85.2 | 37.1-1050 | 1.52-4.33 |
| PL | PL-PX | mean | - | 0.015940.0173 (3) | 0.62040.987 (4) | 2.9344.73 (4) | 1.902.55 (4) | 0.081140.0089 (4) | 403.164 (4) | 9.4344.65 (4) | 48.0412.0 (3) | 84.043.99 (4) | 3.1342.32 (3) | 1.9441.73 (4) |
| | | range | - | <0.01-0.04 | 0.1-1.6 | 0.6-11.0 | 0.4-12.9 | 0.05-0.12 | 168-536 | 4-15 | <20-61 | 80.9-88.1 | 180-620 | 0.85-4.50 |
| PY(6) | DUN | mean | 2.1 (1) | 0.54 (2) | 1.22 (2) | 3.51 (2) | 0.41 (2) | 0.220 (2) | 1810 (2) | 20.9 (1) | 65.1 (2) | 85.4 (2) | 6.56 (2) | 8.57 (2) |
| | | range | - | 0.47-0.61 | 1.2-1.3 | 2.7-4.5 | 0.2-0.7 | 0.22 | 1700-1920 | - | 65-70 | 83.3-87.4 | 4.49-9.57 | 6.43-11.4 |
| HAR | mean | - | 0.349 (2) | 1.85 (2) | 1.63 (2) | 1.41 (2) | 0.135 (2) | 1120 (2) | 31.0 (2) | 91 (1) | 86.2 (2) | 46.2 (2) | 12.0 (2) | - |
| | | range | - | 0.20-0.61 | 1.2-2.8 | 1.5-9.17.9 | 0.9-2.1 | 0.13-0.14 | 1010-1280 | 8-20 | - | 86.0-86.4 | 29.3-79.3 | 8.32-16.9 |
| PP(2) | DUN | mean | - | 0.29240.496 (3) | 4.33340.208 (3) | 7.2964.37 (3) | 1.12340.404 (3) | 0.06640.0451 (3) | 1830.310 (3) | 3.16 (2) | 60.0414.0 (3) | 86.741.47 (3) | 7.8748.24 (3) | 6.5045.73 (3) |
| | | range | - | 0.61-1.36 | 4.1-4.3 | 3.3-11.2 | 0.8-1.6 | 0.03-0.12 | 1490-2100 | <1-5 | 51-77 | 83.8-88.4 | 2.12-18.4 | 2.06-13.1 |
| HAR | mean | - | 0.123 (2) | 1.27 (2) | 3.39 (2) | 0.861 (2) | 0.131 (2) | 1520 (2) | 42.2 (2) | 63.4 (2) | 88.0 (2) | 28.7 (2) | 4.17 (2) | - |
| | | range | - | 0.04-0.39 | 0.5-3.3 | 1.1-11.4 | 0.4-1.9 | 0.09-0.19 | 1170-1870 | 25-71 | 59-68 | 87.4-88.6 | 28.3-29.2 | 2.90-6.00 |
| TR(OC) | mean | 0.592 (2) | 0.37840.119 (4) | 2.8131.39 (3) | 3.5540.988 (4) | 1.4240.125 (4) | 0.063940.083 (4) | 1210.330 (4) | 13.748.02 (3) | 49.441.8.5 (4) | 86.940.907 (4) | 9.4046.3.6 (4) | 2.5040.622 (4) | |
| | | range | - | 0.24-0.53 | <1.0-4.6 | 2.6-4.8 | 1.3-1.6 | 0.03-0.21 | 830-1690 | <1-23 | 31-76 | 86.2-88.2 | 6.67-20.0 | 1.86-5.15 |
| PL | HAR | mean | - | 0.28 (1) | 1.3 (1) | 6.6 (1) | 1.08 (1) | 0.16 (1) | 1110 (1) | 17 (1) | 213 (1) | 84.8 (1) | 23.6 (1) | 0.61 (1) |
| | | range | - | 0.15240.146 (4) | 1.2131.27 (4) | 6.952.89 (4) | 6.282.78 (4) | 0.27040.0956 (4) | 943.302 (4) | 33.027.6 (4) | 49.640.9 (3) | 84.341.34 (4) | 4.5-949.18 (4) | 1.1140.469 (4) |
| PL | LHER | mean | - | 0.05-0.24 | 0.7-3.4 | 4.6-10.5 | 4.1-10.3 | 0.19-0.42 | 562-1300 | 11-77 | <20-104 | 83.2-86.2 | 14.8-21.0 | 0.73-1.83 |
| | | range | - | 0.51-1.15 | 3.6-7.2 | 3.3-9.1 | 0.3-1.0 | 0.07-0.16 | 1170-2850 | <1-10 | <20-132 | 84.3-91.5 | 4.32-17.8 | 5.73-22.0 |
| BH | DUN | mean | - | 0.68140.238 (3) | 5.341.40 (3) | 5.682.21 (3) | 0.54540.292 (3) | 0.110740.0370 (3) | 2160.474 (8) | 27.134.37 (6) | 83.844.2 (7) | 88.142.26 (8) | 5.2546.33 (3) | 10.444.36 (3) |
| | | range | - | 0.34-1.15 | 3.6-7.2 | 3.3-9.1 | 0.3-1.0 | 0.07-0.16 | 1170-2850 | <1-10 | <20-132 | 84.3-91.5 | 4.32-17.8 | 5.73-22.0 |
| HAR | mean | 0.425 (2) | 0.34640.240 (10) | 2.8431.37 (10) | 9.9346.68 (10) | 1.162.89 (10) | 0.07180.0488 (10) | 1570.917 (10) | 5.535.56 (8) | 78.541.04 (10) | 87.342.57 (10) | 27.1231.5 (10) | 8.202.22.1 (10) | |
| | | range | - | 0.13-0.89 | 1.1-5.3 | 5.1-21.2 | 0.1-9.9 | 0.02-0.15 | 1200-2250 | <1-31 | 30-384 | 82.3-91.1 | 6.64-98.6 | 2.09-74.3 |
| OPX + | WZB | mean | 0.8 (1) | 0.14040.0945 (2) | 1.3441.37 (6) | 14.0213.3 (6) | 1.4440.891 (6) | 0.12140.0729 (6) | 663.133 (7) | 10.2421.9 (7) | 140.78.5 (9) | 89.441.04 (7) | 100.57.9 (6) | 9.743.20.3 (6) |
| | | range | - | 0.03-0.32 | 0.2-3.7 | 4.0-42.6 | 0.3-2.9 | 0.07-0.25 | 368-1130 | 4-65 | <20-268 | 87.5-94.2 | 57.5-213 | 9.743.20.3 (6) |
| TR(OC) + | ANOR | mean | 2.3 (1) | 0.27140.401 (5) | 3.1730.497 (4) | 5.3733.07 (5) | 1.5440.723 (3) | 0.12540.0472 (5) | 837.474 (5) | 11.646.66 (3) | 163.84.6 (3) | 87.643.77 (5) | 19.841.6.3 (5) | 3.4942.17 (5) |
| | | range | - | 0.09-1.09 | <0.3-3.8 | 2.8-9.7 | 0.6-2.5 | 0.06-0.18 | 34-1270 | <1-19 | <20-271 | 85.3-94.2 | 7.61-48.5 | 1.12-6.06 |
| PL | HAR | mean | - | 0.150 (2) | 0.901 (2) | 4.30 (2) | 2.27 (2) | 0.489 (2) | 912 (2) | 60.7 (2) | 212 (2) | 83.8 (2) | 28.7 (2) | 1.89 (2) |
| | | range | - | 0.07-0.22 | 0.8-1.0 | 2.8-6.6 | 0.5-10.1 | 0.31-0.77 | 127-1290 | 46-80 | 163-277 | 82.0-85.5 | 8.51-93.6 | 0.65-5.53 |
| PL | OPX | mean | - | 0.100 (2) | 2.3 (1) | 4.31 (2) | 2.45 (2) | 0.107 (2) | 438 (2) | 8.49 (2) | - | 87.2 (2) | 4.1 (2) | 1.78 (2) |
| | | range | - | 0.10 | 2.3 (1) | 2.2-8.6 | 1.3-4.6 | 0.05-0.23 | 284-592 | 4-18 | - | 84.7-89.7 | 22.0-86.0 | 0.48-6.62 |

APPENDIX 2. PRECIOUS METAL, TRACE ELEMENT AND SPINEL ANALYSES FOR TRAVERSE A-A', HEAZLEWOOD RIVER COMPLEX

| Sample # | Distance | Sequence | Rock Type | Os | Ir | Ru | Pt | Pd | Au | Ni | Cu | S | Mg# | Cr* | Al* | Fe3+* |
|----------|----------|----------|-----------|------|------|------|------|------|------|------|----|-----|------|------|------|-------|
| 17 | 300 | NM | DUNITE | 2.1 | 0.87 | 2.2 | 0.4 | nd | 0.02 | 2450 | 8 | 45 | 93.8 | 13.8 | 2.01 | 0.13 |
| 18 | 400 | NM | DUNITE | nd | 0.52 | 4.4 | 0.2 | 0.9 | 0.16 | 2600 | 13 | 48 | 94.0 | nd | nd | nd |
| 351 | 405 | NM | DUNITE | nd | 0.99 | 4.0 | 0.5 | 0.2 | 0.09 | 2480 | 2 | <20 | 93.2 | 15.0 | 0.72 | 0.10 |
| 19 | 420 | NM | DUNITE | 10.2 | 1.92 | 2.8 | 14.9 | nd | 0.05 | 2800 | 9 | 49 | 90.6 | nd | nd | nd |
| 20 | 430 | NM | DUNITE | 8.4 | 3.29 | 5.2 | 0.2 | nd | 0.06 | 2470 | 1 | 33 | 92.8 | 14.5 | 1.39 | 0.06 |
| 340 | 460 | NM | DUNITE | nd | 3.91 | 9.5 | 4.6 | 1.0 | 0.14 | 2550 | 8 | <20 | 92.3 | 14.9 | 0.96 | 0.01 |
| 23 | 470 | NM | DUNITE | 34 | 5.09 | 7.8 | 7.8 | nd | 0.11 | 2530 | 6 | 29 | 92.4 | 14.4 | 1.36 | 0.12 |
| 24 | 500 | NM | DUNITE | 4.4 | 3.20 | 8.4 | 0.3 | nd | 0.06 | 2580 | 2 | 33 | 92.8 | 14.3 | 1.48 | 0.13 |
| 341 | 520 | NM | OPX | nd | 0.21 | 1.7 | 8.5 | 0.1 | 0.32 | 628 | 8 | <20 | 83.7 | 9.71 | 3.75 | 2.46 |
| 342 | 570 | NM | DUNITE | nd | 0.02 | 2.6 | 2.4 | 0.8 | 0.13 | 1890 | 10 | <20 | 88.7 | 11.2 | 3.92 | 0.78 |
| 343 | 580 | NM | OPX | nd | 0.10 | 3.9 | 8.1 | 0.7 | 0.15 | 796 | 13 | <20 | 87.3 | 14.3 | 1.27 | 0.37 |
| 25 | 615 | NM | HARZ | 1.4 | 0.28 | 0.7 | 4.8 | nd | 0.30 | 1190 | 4 | 105 | 86.4 | 13.6 | 1.96 | 0.33 |
| 26 | 620 | NM | OPX | 1.5 | 0.30 | 4.2 | 5.2 | nd | 0.17 | 668 | 2 | 26 | 87.6 | 14.2 | 1.29 | 0.46 |
| 344 | 630 | NM | DUNITE | nd | 0.32 | 4.9 | 4.8 | 1.2 | 0.17 | 2030 | 15 | <20 | 89.9 | 10.8 | 4.54 | 0.57 |
| 345 | 700 | NM | DUNITE | nd | 0.27 | 3.1 | 6.2 | 0.6 | 0.14 | 2160 | 5 | <20 | 91.7 | 13.4 | 2.29 | 0.22 |
| 347 | 720 | NM | DUNITE | nd | 0.79 | 3.3 | 0.4 | 0.3 | 0.10 | 2540 | 4 | <20 | 92.8 | 14.9 | 0.96 | 0.12 |
| 27 | 760 | NM | OPX | <0.9 | 0.35 | 0.7 | 3.6 | nd | 0.19 | 1160 | 2 | 27 | 88.3 | 11.8 | 1.89 | 2.27 |
| 348 | 770 | NM | DUNITE | nd | 0.51 | 4.6 | 4.2 | 0.6 | 0.27 | 1930 | 13 | <20 | 90.4 | 13.9 | 1.75 | 0.38 |
| 349 | 820 | NM | DUNITE | nd | 0.91 | 4.3 | 1.9 | 0.3 | 0.13 | 2710 | 11 | <20 | 91.8 | 13.4 | 2.23 | 0.33 |
| 28 | 850 | NM | OPX | 1.3 | 0.30 | <0.4 | 7.0 | nd | 0.44 | 750 | <1 | 25 | 87.6 | 11.7 | 2.78 | 1.44 |
| 350 | 870 | NM | DUNITE | nd | 0.25 | 2.9 | 2.6 | 0.5 | 0.10 | 1810 | 2 | 35 | 88.9 | 13.3 | 2.27 | 0.31 |
| 352 | 900 | NM | DUNITE | nd | 0.63 | 3.8 | 0.5 | 0.3 | 0.12 | 2640 | 9 | 23 | 93.2 | 14.3 | 1.41 | 0.16 |
| 29 | 930 | FS | OPX | 0.9 | 0.32 | 0.8 | 3.0 | nd | 0.45 | 798 | <1 | 29 | 85.0 | 10.3 | 3.31 | 2.28 |
| 30 | 1010 | FS | OPX | 0.9 | 0.32 | 2.1 | 2.6 | nd | 0.10 | 887 | 2 | 26 | 88.1 | 11.1 | 2.60 | 2.23 |
| 31 | 1100 | FS | OPX | 0.9 | 0.33 | 1.1 | 5.7 | nd | 0.56 | 796 | <1 | 24 | 87.9 | 10.7 | 2.74 | 2.44 |
| 32 | 1150 | FS | OPX | 1.5 | 0.35 | 1.8 | 5.0 | nd | 0.28 | 788 | 4 | 54 | 85.9 | 10.0 | 3.07 | 2.83 |
| 33 | 1160 | FS | OPX | nd | 0.21 | 1.2 | 5.3 | nd | 0.08 | 805 | 2 | 29 | 85.7 | 10.2 | 2.90 | 2.87 |
| 37 | 1200 | FS | OPX | nd | 0.20 | 1.6 | 5.3 | nd | 0.03 | 839 | 2 | 31 | 88.0 | 11.0 | 2.74 | 2.24 |
| 34 | 1260 | FS | OPX | nd | 0.16 | 0.9 | 7.5 | 0.1 | 0.05 | 813 | 3 | 28 | 84.7 | 9.77 | 3.26 | 2.93 |
| 35 | 1320 | FS | OPX | nd | 0.11 | 2.0 | 2.9 | 0.3 | 0.07 | 848 | 4 | 21 | 84.5 | 12.3 | 1.76 | 1.92 |
| 38 | 1360 | CH | OPX | nd | 0.19 | 1.6 | 1.8 | 0.2 | 0.04 | 1200 | 4 | <20 | 87.6 | 11.6 | 2.16 | 2.09 |
| 39 | 1365 | CH | DUNITE | nd | 0.22 | 0.9 | 2.5 | <0.3 | 0.03 | 1560 | 2 | 24 | 90.4 | 11.8 | 2.02 | 2.08 |
| 40 | 1450 | CH | OPX | nd | 0.15 | 2.6 | 0.7 | <0.5 | 0.04 | 1050 | 1 | 58 | 89.9 | 12.1 | 2.10 | 1.74 |
| 41 | 1455 | CH | DUNITE | nd | 0.15 | 2.4 | 9.2 | 0.4 | 0.04 | 2060 | 4 | 184 | 87.1 | 10.1 | 2.82 | 3.03 |
| 36 | 1580 | CH | OPX | nd | 0.20 | 1.4 | 5.2 | 2.2 | 0.11 | 928 | 31 | <20 | 83.3 | nd | nd | nd |
| 42 | 1700 | CH | OPX | nd | 0.17 | 1.5 | 3.9 | 0.8 | 0.04 | 631 | 3 | 52 | 83.4 | 7.80 | 4.18 | 3.81 |
| 43 | 1900 | CH | HARZ | nd | 0.22 | 1.5 | 1.2 | <0.4 | 0.04 | 1790 | 3 | 45 | 86.7 | 8.04 | 4.69 | 3.19 |
| 44 | 2200 | CH | OPX | nd | 0.19 | 1.1 | 3.6 | 0.1 | 0.08 | 699 | 5 | 42 | 82.8 | 6.62 | 4.61 | 4.52 |
| 493 | 2330 | CH | OPX | nd | nd | nd | nd | nd | nd | 624 | 27 | <20 | 82.0 | 7.41 | 4.51 | 3.98 |
| 489 | 2420 | CH | OPX | nd | nd | nd | nd | nd | nd | nd | nd | nd | nd | 9.15 | 5.82 | 0.95 |
| 45 | 2450 | CH | OPX | nd | 0.16 | 3.4 | 4.8 | 0.4 | 0.07 | 634 | 10 | 42 | 81.3 | 6.43 | 2.85 | 6.56 |
| 490 | 2580 | CH | OPX | nd | nd | nd | nd | nd | nd | 598 | 15 | <20 | 82.8 | 7.41 | 4.42 | 4.02 |
| 494 | 2620 | CH | OPX | nd | nd | nd | nd | nd | nd | 841 | 13 | <20 | 85.1 | 6.87 | 3.58 | 5.35 |
| 46 | 2650 | CH | OPX | nd | 0.09 | <0.6 | 4.1 | 0.2 | 0.07 | 684 | 5 | 44 | 83.4 | 7.16 | 3.30 | 5.27 |
| 491 | 2720 | CH | PL. OPX | nd | nd | nd | nd | nd | nd | nd | nd | nd | nd | 5.08 | 2.19 | 8.50 |
| 492 | 2780 | CH | PL. LHERZ | nd | nd | nd | nd | nd | nd | 212 | 22 | 23 | 72.7 | 0.98 | 1.35 | 12.7 |
| 47 | 2900 | CH | PL. OPX | nd | 0.10 | 0.8 | 4.6 | 0.4 | 0.10 | 663 | 1 | 74 | 83.1 | 5.89 | 2.25 | 7.75 |
| 228 | 3000 | CH | PL. OPX | nd | 0.12 | 0.4 | 9.7 | 0.8 | 1.89 | 516 | 12 | 56 | 79.8 | 4.17 | 1.52 | 10.0 |

Notes: PGE and Au are reported in ppb, trace elements are in ppm. Distance refers to the relative position (in m) of the samples from west to east, along Traverse A (see Figure 2). Spinel atomic proportions are indicated by *, and are derived from averages of three to eight spot analyses based on 24 cations and 32 oxygens. Abbreviations: NM-Nineteen Mile Creek Sequence; FS-Fenton's Spur Sequence; CH-Caudry's Hill Sequence; OPX-orthopyroxenite; HARZ-harzburgite; PL.-plagioclase; LHERZ-lherzolite; nd-not determined.